Effect of Low Voltage on the Aging of Fuel Cells

A Major Qualifying Project
Report submitted to the
faculty of
WORCESTER POLYTECHNIC INSTITUTE
in partial fulfillment of the requirements
for the Degree of Bachelor of Science

Submitted to:
Professor Stephen Kmiotek

By:

Sarah Kapelner
Mercedes Kuzina

March 28th 2015

Co-Advised by:

Caroline Bonnet (ENSIC)
Francois Lapique (ENSIC)

Abstract

Proton exchange membrane fuel cells (PEMFC) are an attractive source of current in many applications when coupled with supercapacitors. Supercapacitors operate via several charge and discharge cycles. When a supercapactitor is discharged, or at near zero voltage, the fuel cell must work at near zero voltage to supply the current. The effects of low voltage operation on the aging of PEMFCs are widely unknown. This major qualifying project conducted at ENSIC in Nancy, France, seeks to investigate these effects by studying the degradation of a PEMFC operating at low voltage. This experiment achieved low voltage operation by short-circuiting the fuel cell using a copper bracket. The cell operated for a total of six weeks where weekly characterization tests were conducted to evaluate the health of the membrane. The degradation of the fuel cell MEA was characterized by polarization curves, impedance spectroscopy, linear sweep voltammetry, and cyclic voltammetry.

Research determined that over the course of the experiment the performance of the fuel cell decreased. However, voltammetry testing indicated that the membrane and catalyst layer degraded little over the course of six weeks.

It is recommended to continue investing the lifetime of the MEA at low voltage operation. In future experiments, other characterization tests should be conducted weekly to monitor the performance of other aspects of the fuel cell such as electrodes and gas diffusion layers.

Table of Contents

Table of Figures

Table of Tables

Nomenclature

CV	cyclic voltammetry
E	potential (V)
E_o	standard thermodynamic voltage (V)
ECSA	electrochemical catalyst surface area (cm^2 Pt/g Pt)
EIS	electrochemical impedance spectroscopy
F	Faraday's constant (96,485 C mol^{-1})

I	fuel cell current (A)
i	fuel cell current density (A cm^{-2})
i_{H2}	hydrogen crossover current
LSV	linear sweep voltammetry
n	reactant stoichiometric coefficient
na	constant phase element parameter at anode
nc	constant phase element parameter at cathode
OCV	open circuit voltage
P	atmospheric pressure (101,325 kPa)
P_d	power density
PEMFC	proton exchange membrane fuel cell
Q_a	pseudo capacitance anode
Q_c	pseudo capacitance cathode
Q_i	volumetric flow rate (L s^{-1})
Q_v	flow of hydrogen crossover
R	gas constant (J mol^{-1} K^{-1})
R_a	charge transfer resistance at anode
R_c	charge transfer resistance at cathode
R_{ct}	charge transfer resistance
R_d	diffusion resistance
R_{sc}	Short circuit resistance
$R_{\mathbf{w}}$	Ohmic resistance
T	temperature (K)
V	fuel cell voltage (V)
Z’	real impedance
Z’’	imaginary impedance

Greek Symbols

α	charge transfer coefficient for redox reaction
β	charge transfer coefficient for redox reaction
l	flow meter correction factor
γ	activity of reacting species
ν_i	stoichiometric coefficient of species i

Acknowledgements

We would like to thank ENSIC for their partnership and collaboration on this project. A special acknowledgment to Francois Lapicque, Caroline Bonnet and Stephen Kmiotek for their guidance, knowledge, and support throughout the duration of this project.

Background

Introduction

A fuel cell is a device that converts chemical energy into electrical energy via several electrochemical reactions. Fuel cell technology has the ability to significantly reduce the amount of pollutants, such as green house gases in the atmosphere compared to traditional combustion-based power generation technologies. In addition, fuel cells have the advantage of being more efficient compared to traditional combustion engines because a fuel cell is not restricted by the Carnot limitation.

A fuel cell generates electricity, heat and water via an irreversible electrochemical reaction. The overall chemical reaction for generating electricity is:

$$\frac{1}{2}O_2 + H_2 \rightarrow H_2O$$

All fuel cells are comprised of two porous carbon electrodes: a positively charged anode and negatively charged cathode. At the anode, hydrogen is oxidized to form protons via the following oxidation reaction:

$$H_2 \rightarrow 2H^+ + 2e^-$$

At the cathode, oxygen reacts with electrons taken from the electrode and the H^+ irons from the electrolyte to form water. Below is the reduction reaction that occurs at the cathode:

$$\frac{1}{2}O_2 + 2H^+ + 2e^- \rightarrow H_2O$$

Both of these reactions proceed continuously and electrons that are produced at the anode must pass through the electrical circuit to the cathode, which produces a current or "load". In addition, H^+ ions must pass through the electrolyte (Larminie & Dicks, 2003). The potential of the cell is limited by the two-redox

reactions. The change linked to oxidation and the anode is equal to 0 V, but the change linked to reduction at the cathode produces 1.23 V. However, due to several resistances this fuel cell potential is unobtainable (Lapicque, 2015).

Types of Fuel Cells

The main disadvantages of fuel cells include the slow reaction rates as well as the availability of hydrogen. A slow reaction rate is overcome by the application of a highly porous electrode with a platinum catalyst and/or operating at a high pressure. Hydrogen is more regarded as an energy carrier rather than an energy source because it is not found naturally in a pure uncombined form. Hydrogen is also difficult to store and transport.

These disadvantages have resulted in the manufacturing of several different types of fuel cells. The six different types of fuel cells are typically differentiated by the electrolyte used and the operating temperature range (Larminie & Dicks, 2003) Basic information regarding the various types of fuel cells is summarized in Table 1 on the following page.

Fuel Cell Type	Electrolyte	Operating Temperature (°C)	Applications
Alkaline (AFC)	KOH	50-200	Space vehicles
Proton exchange membrane (PEMFC)	Polymer	30-100	Vehicle and mobile applications Low power CHP systems
Direct Methanol (DMFC)	Polymer	20-90	Low power portable electronics
Phosphoric Acid (PAFC)	Phosphoric Acid	~220	High power CHP Systems
Molten carbonate (MCFC)	Molten Carbonate	~650	Medium to high power CHP Systems
Solid oxide (SOFC)	Solid Oxide	500-1000	Suitable all power CHP systems

Table 1: Various types of Fuel cells and their applications

Proton Exchange Membrane Fuel Cell

The proton exchange membrane fuel cells (PEMFC) are the simplest and most widespread fuel cells in the automotive and mobile appliance industry due to their efficiency, power density, and durability (Larminie & Dicks, 2003).

History of Proton Exchange Membrane Fuel Cells

General Electric developed the first PEMFC, also known as the *solid polymer fuel cell*, in the 1960's for NASA. However, an issue of water management in the electrolyte resulted in NASA utilizing the alkaline fuel cell in their spacecraft's. At this time, GE did not pursue commercializing the PEMFC due to the cost being higher than other fuels cells, such as the Phosphoric Acid fuel cell. The further development of the PEMFC went

stagnant during most of the 1970s and 1980s. However toward the late 1980's and early 1990's, Ballard Power Systems began to research and improve PEMFC technology. Their developments were able to increase the current densities of the fuel cell, while also reducing the use of platinum by a factor of 100, from 28 $\frac{mg}{cm^2}$ to .2 $\frac{mg}{cm^2}$. As a result of these advances, PEMFC are now a preferred option for NASA spacecraft's. It can be argued that PEMFC's exceed all other electrical generating technologies with the broad scope of their applications. Research is being conducted to apply PEMFC technology to automobiles, mobile phones, computers, boats, busses, and industrial equipment (Larminie & Dicks, 2003).

Fundamentals of the PEMFC

A PEMFC consists of several layers that all serve a unique purpose in the operation of the fuel cell. The assembly and characteristics of each layer facilitate the flow of reactants and products, which result in the creation of electrical energy. Figure 1 on the following page demonstrates the various layers of a single fuel cell manufactured by UBzM in Germany.

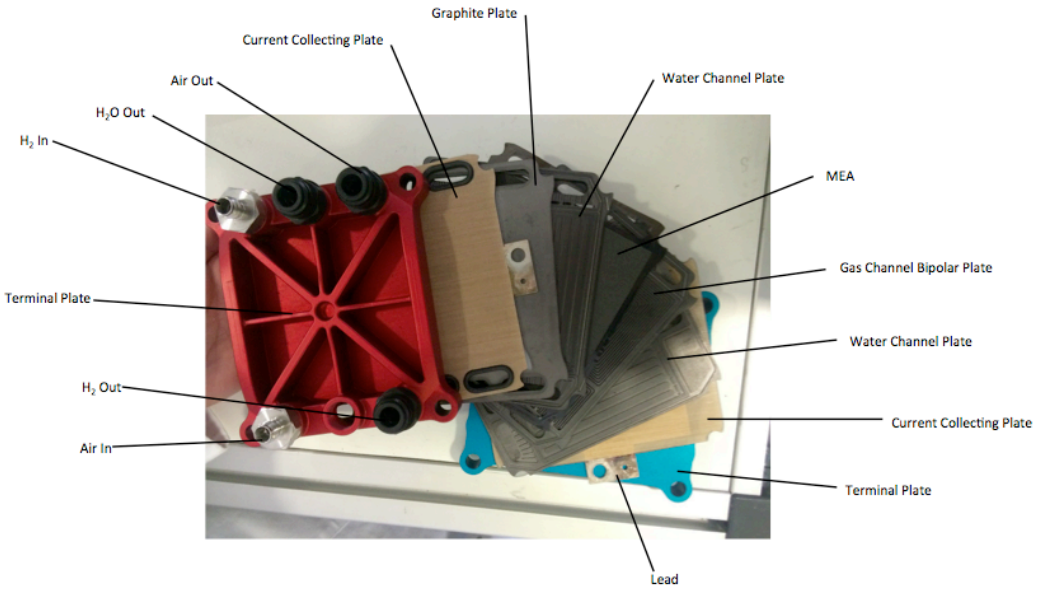

Figure 1: Layered components of a single PEMFC from UBzM Germany

A fuel cell consists of two different parts: the plates and the membrane electrode assembly (MEA). The plates include end plates, current collecting plates and flow plates. The MEA contains several layers, namely the gas diffusion layers (GDLs), two electrodes and an electrolyte membrane.

Plates

The outermost plates of the fuel cell are called the end plates, which hold the cell together. These plates have inlet and outlet openings to allow for the flow of hydrogen, oxygen, and water. Following the endplates on either side are the current collecting plates, which collect and conduct electron flow from the electrodes. The current collecting plates also have a contact lead to establish an external circuit. Following the current collecting plates are the channel plates, which are comprised of carbon and polymer based materials. The unique patterns and ducts in the channel plates direct the flow of water and oxygen. Channel plates can either be double-sided or single-sided. In a double-sided channel plate, the gas flow channel is located on one side and the water

flow channel on the other. In a single-sided channel plate, two channel plates are needed: one to direct gas flow and the other to direct water flow. The gas channel plates serve to distribute the gases onto the MEA. The water channel plates regulate the temperature of the cell and also allow electrical contact between the final plate and the catalyst layers. In a fuel cell stack, it is necessary to have two single-sided channel plates to direct the flow of water and one double-sided gas channel plate, also known as bipolar plate, which has flow patterns for gases on either side to direct the flow of hydrogen to the anode and oxygen to the cathode (Larminie & Dicks, 2003).

Membrane Electrode Assembly

The membrane electrode assembly (MEA) is the core component of a fuel cell. The MEA is composed of gas diffusion layers (GDLs), electrodes, and a polymer electrolyte membrane (PEM). The figure below depicts a typical MEA used in a PEM fuel cell.

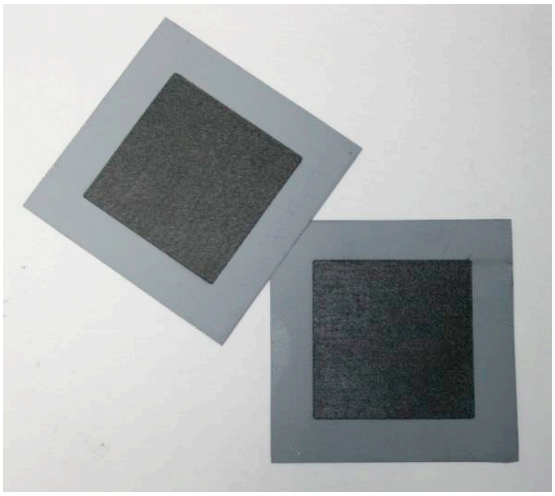

Figure 2: Example of a membrane electrode assembly (MEA)(Paxi Tech,2015)

The MEA can be assembled via two different processes: the separate electrode method and the direct method. In the separate electrode method, each electrode is adhered to a GDL then each assembly is hot pressed on to either side of the PEM. In the

direct method, the electrode is built directly onto the electrolyte. Both methods yield the equivalent MEA construction. The layout of an MEA is depicted in Figure 3 below:

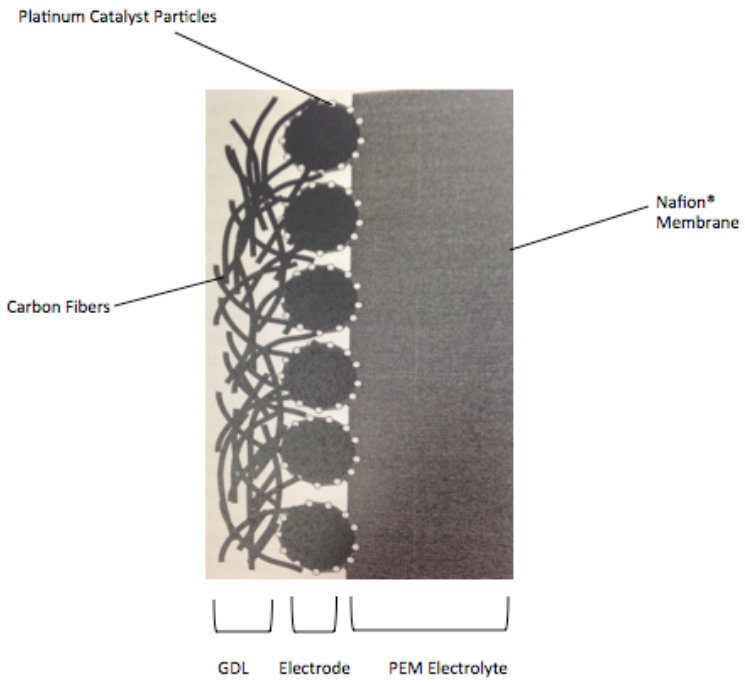

Figure 3: MEA Component Assembly (Larminie & Dicks, 2003)

The outermost layer of the MEA is the gas diffusion layer GDL. The GDL joins the electrode with the current collecting plate. These layers located on both sides of the MEA, allow gas access from the fluid flow channel to the catalyst layer and also allow removal of gaseous products. In addition, the GDL also provides a passage for water removal from the electrode to the flow field. The GDL had a high electrical and heat conductivity and is comprised of carbon paper, which provides protection and mechanical support to the inner MEA (Hartnig & Roth, 2012; Larminie & Dicks, 2003).

Every fuel cell has two electrodes, which are termed the anode and cathode. The anode and cathode are located on either side of the electrolyte membrane and are the

locations in which the oxidation and reduction half reactions occur. Both half reactions are catalyzed by platinum particles fixed on finely divided carbon powder.

Between both electrodes, is the electrolyte layer, which is theoretically impermeable to electrons and porous to the transportation of water and protons. The electrolyte layer is the central aspect of the PEMFC. Most membranes are composed of a sulphonated fluoropolymer. Figure 4 below, is an example of a sulphonated fluoroethylene polymer. The most common and well known is Nafion®, which is produced by DuPont.

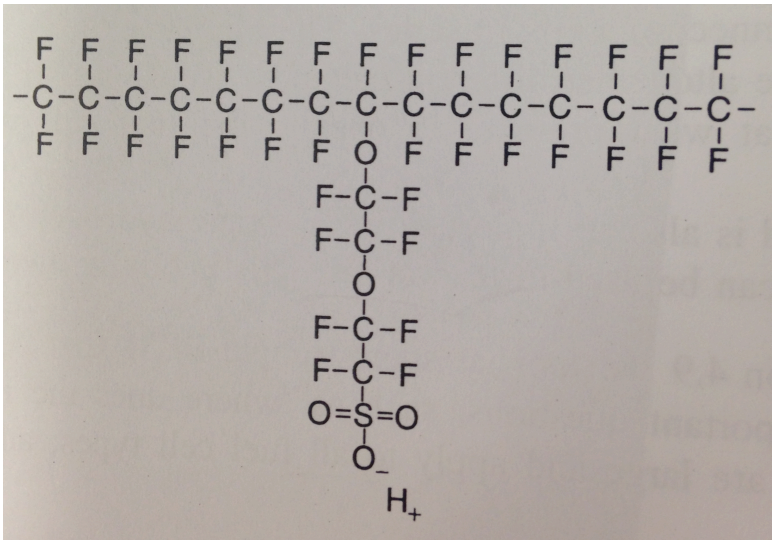

Figure 4: Example structure of a sulphonated fluoroethylene (Larminie & Dicks, 2003)

The polymer electrolyte membrane is produced using polyethylene, but substituting fluorine for hydrogen modifies its structure. This modified polymer is called polytetrafluoroethylene, or PTFE. The bonds between fluorine and carbon are strong, which make the membrane durable and resistant to chemical attack. In addition, the carbon-fluorine bonds are highly hydrophobic, which removes water from the electrode and prevents flooding of the fuel cell. Sulphonic acid, HSO_3, is added as a side-chain on the PTFE polymer. This sulphonic acid side chain is highly hydrophilic, which results in large consumptions of water. In these hydrated regions, the protons are slightly attracted

to the SO_3^- resulting in a conductive dilute acid where protons can move freely. Overall, the electrolyte membrane is comprised of dilute acid regions surrounded by tough hydrophobic structure (Larminie & Dicks, 2003).

Application of Faradays Law

The necessary reactant flow rates needed to achieve a desired current were calculated using the following form of Faraday's Law:

$$Q = \frac{I}{n*F} * \frac{RT}{P} \qquad (1)$$

Where Q (L/s) is the reactant flow rate, I (A) is the current, F is Faraday's constant, R is ideal gas constant, T (K) temperature, P (Kpa) pressure and n is the reactant stoichiometric coefficient. The reactant stoichiometric coefficient for hydrogen and oxygen were determined given by the following overall oxidation and reduction reactions:

$$2H_2 \rightarrow 4H^+ + 4e^-$$

$$O_2 + 4H^+ + 4e^- \rightarrow 2H_2O$$

The stoichiometric coefficient value for hydrogen is equal to 2 and for oxygen is equal to 4.

It is preferable to use air instead of pure oxygen since air is more abundant and oxygen reduction is sluggish (Lapicque, 2015). In this case, the equation below yields the flow rate of oxygen given an air composition equal to 21 % oxygen and 79% nitrogen.

$$Q_{O_{2\,in}} = .21 * Q_{air_{in}} \qquad (2)$$

To account for any flow meter error and ensure that both reactants are in excess, the resulting flow rates were multiplied by a correction factor of 1.4 for hydrogen and 2.4 for oxygen. These correction factors ensure a forty percent excess of hydrogen and a one hundred forty percent excess of oxygen in air. Overall, the information derived from Faraday's Law was used to determine the necessary reactant flow rates in order for the fuel cell to supply a specific electrical current (Bonnet, 2014).

Assessment of Fuel Cell Performance

There are several "classical" techniques that can be used to assess the health of fuel cells. Fuel cell performance is, in part, based on the power output of the cell, which can be determined given the following equation:

$$P = I*V \qquad (3)$$

In analyzing and characterizing fuel cell performance it is necessary to use techniques that track both voltage and current. It is also useful to study the charge of hydrogen for during desorption on the platinum catalyst and hydrogen crossover within the cell to evaluate the effectiveness of the catalyst and degradation of the MEA.

Polarization Curves

Polarization curves, plots of cell voltage versus current density, are used to assess fuel cell performance in various ways. One way is to use polarization curves to determine the power output of fuel cells. In addition, several polarization curves recorded at different points in time can be compared to obtain information on fuel cell performance.

Polarization curves are often created under the condition of Open Circuit Voltage (OCV), which is the voltage produced by a fuel cell when there is no electrical load on

the cell (Wang, 2012). The OCV is almost always lower than the theoretical voltage of a fuel cell. The theoretical voltage for a PEMFC is also given by the Nernst Equation:

$$E = E_0 - \frac{RT}{nF} ln \frac{\Pi \gamma_{Products}^{vi}}{\Pi \gamma_{Reactants}^{vi}} \qquad (4)$$

where E_0 is the standard thermodynamic voltage at 25°C, R is the universal gas constant, F is Faraday's constant, γ is the activity of the product or reactant, v_i is the stoichiometric coefficient of species i, n is the electron transfer number for the reaction and T is the absolute temperature (Wang, 2012). The difference between OCV and theoretical voltage is called irreversible voltage loss, which is caused by mass transfer limitations during crossover from the anode to the cathode.

There are different forms of voltage or electric potential losses that occur in the fuel cell at different current density levels. These losses are reflected in polarization curves. The three losses taking place include: activation loss, ohmic loss and mass transport loss. The regions of the polarization curve where each type of loss occurs is evidenced in Figure 5 below.

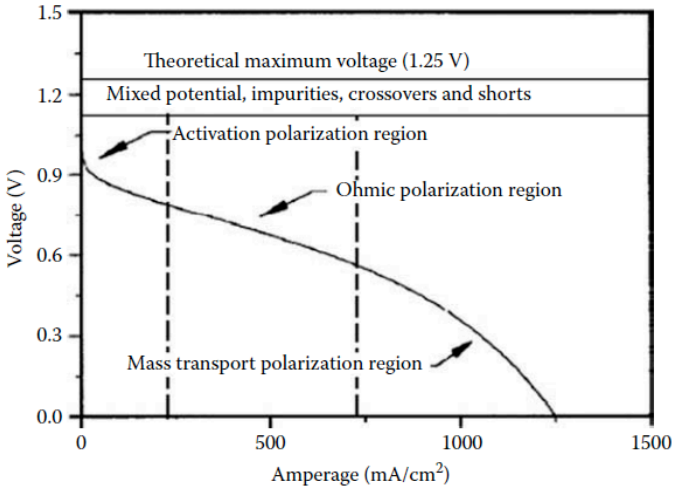

Figure 5: A typical polarization curve showing regions of current at which different voltage losses occur (Wang, 2012).

The vertical distance between the polarization curve and the theoretical maximum voltage is indicative of the power output of the fuel cell. The shorter this distance, the greater the power output. As the cell ages, the polarization curve shifts downward and the power output decreases for all current values. This is indicative of a decrease in fuel cell performance.

Activation losses or charge transfer resistance takes place in the low current density region of the polarization curve. This type of loss is due to sluggish charge transfer at the electrode of the fuel cell during the redox reaction. This type of loss is described by the Butler-Volmer equation:

$$i = i_0 \left\{ \exp\left(\frac{\alpha n F \eta_{act}}{RT} \right) - \exp\left(-\frac{\beta n F \eta_{act}}{RT} \right) \right\} \quad (5)$$

Where α and β are transfer coefficients, i_0 is the exchange current density, i is current density and η_{act} is the activation loss/charge transfer resistance (Wang, 2012).

Irreversible voltage loss is just one type of loss that occurs in PEMFCs. In the intermediate current range of a polarization curve, ohmic losses or ohmic resistance mainly causes the voltage drop. Ohmic resistance consists of the internal resistance of electric contact resistance among fuel cell components, such as an interface connected by a bolt, and proton resistance across the MEA. In a PEMFC the proton resistance plays a greater role in ohmic resistance than electric contact resistance (Wang, 2012).

Mass transport in a PEMFC is comprised of the advection and diffusion of reactants and products. This leads to mass transport loss or diffusion resistance. It occurs in the high current density range of polarization curves and is due to the fact that the amount of reactant that can react is equal to the amount that reaches the platinum catalyst layer in the fuel cell (Wang, 2012). Some common scenarios preventing the reactants

from reaching this layer include: a low concentration gradient, in the case of diffusion, and interference of fluid flow in the case of advection. Diffusion is described by Fick's Law (equation 5) and advection is described by the advection equation (equation 4) shown below:

$$\frac{\partial \emptyset}{\partial t} = D\frac{\partial^2 \emptyset}{\partial x^2} \qquad (5)$$

where $\frac{\partial \phi}{\partial t} = D\,\Delta\phi$ for 2 or more dimensions is the diffusion coefficient and Ø is the concentration of the diffusing species.

$$\frac{\partial \psi}{\partial t} + \nabla \cdot (\psi \mathbf{u}) = \mathbf{0} \qquad (6)$$

where $\nabla \cdot \mathbf{u} = u_x\frac{\partial}{\partial x} + u_y\frac{\partial}{\partial y} + u_z\frac{\partial}{\partial z}$, u is the velocity and ψ is a scalar quantity.
The theoretical voltage losses resulting from mass diffusion are called Nernst Losses, which can be calculated with the following equation:

$$\eta_{conc} = (1 + \frac{1}{\alpha})\frac{RT}{nF} ln \frac{C_R^0}{C_R^*} \qquad (7)$$

where C_R^0 is the bulk concentration of reactant, C_R^* is the concentration of reactant on the catalyst layer and α is a transfer coefficient. In the case of PEMFCs, there will be significant diffusion resistance if hydrogen and air flow is inhibited.

Polarization curves can be recorded under steady-state or transient conditions. In the case of steady-state conditions polarization curves, the voltage or electric potential is recorded as the current is varied. The rate of change of current must be relatively low for

steady-state recording. Alternatively, a polarization curve can be created under transient conditions using a slow current sweep rate (Wang, 2012).

Polarization curves are a widely used technique to assess the power output of fuel cells. However, recording polarization curves is a time-consuming process. For this reason it is preferable to use different techniques, such as those discussed in the following sections.

Electrochemical Impedance Spectroscopy

Electrochemical Impedance Spectroscopy (EIS) is another technique used to study the health of fuel cells. EIS involves obtaining the impedance of a fuel cell and generating a plot called a Nyquist plot, which shows the relationship between the imaginary part of the impedance and the real part of the impedance. EIS gives further information on the three different types of resistance: charge transfer resistance, ohmic resistance and diffusion resistance by providing parameters representing these resistances. In addition, EIS gives parameters for electrode capacitance within the fuel cell (Dandekar and Mandonca, 2012). By analyzing resistance and capacitance values over time information can be obtained on charge transfer, reaction mechanisms, electrode properties and aging/degradation of the fuel cell (Wang, 2012).

Creating a Nyquist plot involves one of two things. Either electric potential (E) is imposed and current (I) is measured over time or I is imposed and E is measured over time. The first method is called Potentiostatic Electrochemical Impedance Spectroscopy (PEIS) and it involves setting the amplitude of the potential, which is a sinusoidal signal. The current response is then measured. Figure 6 on the following page illustrates the imposed sinusoidal potential and the resulting sinusoidal current response that occurs in PEIS. The second method is called Galvanostatic Electrochemical Impedance

Spectroscopy (GEIS) and it involves setting the amplitude of the current and measuring the potential response. Considering PEIS, electric potential is given by Equation 8 as follows:

$$E(t) = E_0 + \Delta E sin(\omega t) \qquad (8)$$

where ΔE is the amplitude of the function *E(t)* and ω is the radial frequency.

I is given by Equation 9 below:

$$I(t) = I_0 + \Delta I sin(\omega t + \theta) \qquad (9)$$

where ΔI is the amplitude of the sinusoidal function, ω is the radial frequency and θ is the phase shift between the *I(t)* and *E(t)* curves shown in Figure 6 below. The phase shift θ is representative of the current response to the electrical potential (Gamry Instruments, 2015). If current were imposed instead of electric potential as in GEIS a similar phase shift would exist in Equation 8 instead of in Equation 9 and on the sinusoidal plot of potential rather than on the sinusoidal plot of current, opposite of what is shown in Figure 6.

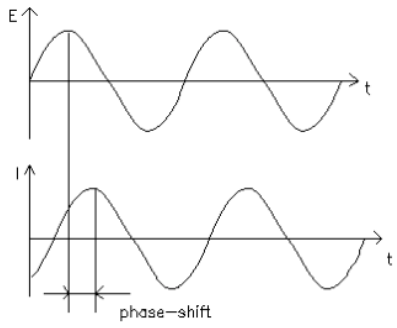

Figure 6: Sinusoidal Response of Current to Electric Potential (Gamry Instruments, 2015)

The phase shift θ and the ratio of electric potential to nominal operating current, $\frac{E}{I}$ are both used in the equation for complex impedance, $Z'' = \frac{Eo}{Io} e^{-j\theta}$, where $j = \sqrt{-1}$. The Real

impedance Z' is obtained by taking the ratio of AC voltage to AC current. Values of impedance at different frequencies, $f=\frac{\omega}{2\pi}$, make up a Nyquist plot (Shudmacher, 2012).

Once the values of Z' and Z'' have been obtained a Nyquist plot can be created. An example of a Nyquist plot is shown in Figure 7 below. The opposite of the imaginary part of the impedance is plotted versus the real part of the impedance and the frequency decreases from left to right.

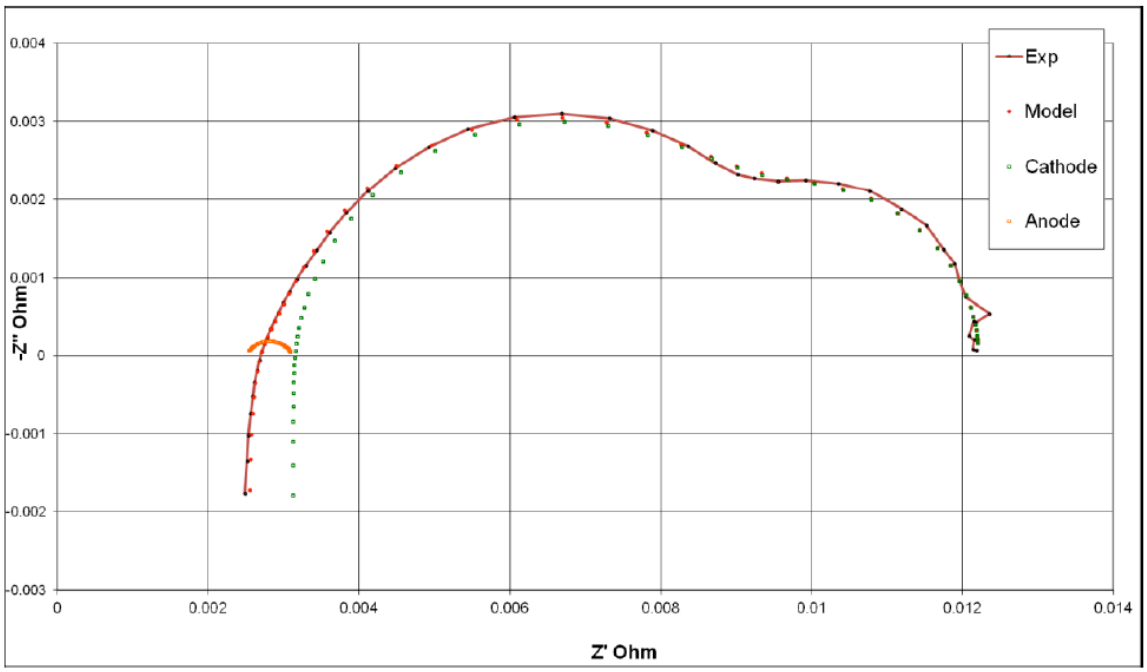

Figure 7: A Nyquist plot (Dandekar and Mandonca, 2012).

A Nyquist plot can be divided into three areas that represent the three losses previously discussed: activation losses, ohmic losses and mass transport losses.

The leftmost loop, or higher frequency loop, is the region of the plot that describes the activation losses or charge transfer resistance. The second loop, or lower frequency loop, describes mass transport losses or diffusion resistance (Torrents, Mason and Garboczi, 2000). Ohmic losses or ohmic resistance is also represented on the Nyquist plot as the distance from the origin to the point at which the spectra crosses the x-axis

(Dandekar and Mondonca, 2012). Although not typically shown on Nyquist plots, frequencies increase along the x-axis (Vermeeren and Michiels, 2011).

For simple processes where the impedance consists only of the charge transfer resistance (R_{ct}), ohmic resistance (shown as electrolyte resistance in Figure 8 below, R_{el}) and double layer capacitance (C_{dl}) the impedance calculation is simple. R_{ct} can be taken directly from the Nyquist plot as the diameter of one of the loops. Figure 8 shows where R_{ct} and R_{el} can be found on the Nyquist plot. The maximum frequency, f_{max}, can also be taken from the Nyquist plot.

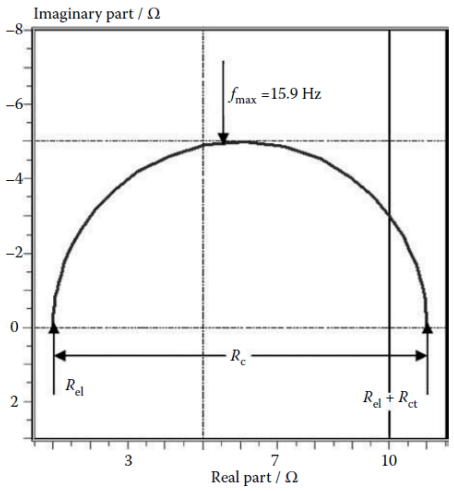

Figure 8: A Nyquist plot with maximum frequency, charge transfer resistance and electrolyte resistance shown. (Wang, 2012)

With R_{ct} and $f_{max,}$ the double layer capacitance, C_{dl}, can be determined from the equation:

$$2\pi f_{max} = \omega_{max} = \frac{1}{C_{dl} R_{ct}} \qquad (10)$$

These values for resistance and capacitance can then be used in analysis of fuel cell performance.

The above method is not sufficient to calculate the impedance for more complicated processes where impedance consists of more than just the charge transfer resistance, ohmic resistance and capacitive phenomena. For these processes it is

necessary to use software that calculates the impedance (Wang, 2012). Then the resulting Nyquist plot is fitted to a model to obtain parameters for resistance and capacitance (Dandekar and Mandonca, 2012).

Electrochemical Impedance Spectroscopy is a widely used technique for analyzing the performance of fuel cells. It is a non-invasive, steady-state technique that gives a wide range of information on fuel cell characteristics. EIS is a well-established technique in studying single fuel cells, under both load and OCV (Dandekar and Mandonca, 2012). Lastly, EIS is an emerging technique for studying stacks of fuel cells (Wang, 2012).

Cyclic voltammetry (CV)

Cyclic Voltammetry (CV) is a widely used technique to obtain qualitative information regarding the fuel cell catalyst and the electrochemical reactions occurring within the MEA (Andrienko, Denis, 2003). CV tests are conducted with hydrogen being fed to the cathode and an inert gas being fed to the anode. This electro-analytical technique is based on linear voltage sweeps between an initial value, V_2, to a predetermined potential limit, V_1, where the direction of the scan is reversed. These linear sweeps between V_1 and V_2 are repeated for a specific duration of time. (Gouws, Shawn. 2012). The linear voltage sweeps in a CV scan are illustrated in Figure 9 on the following page.

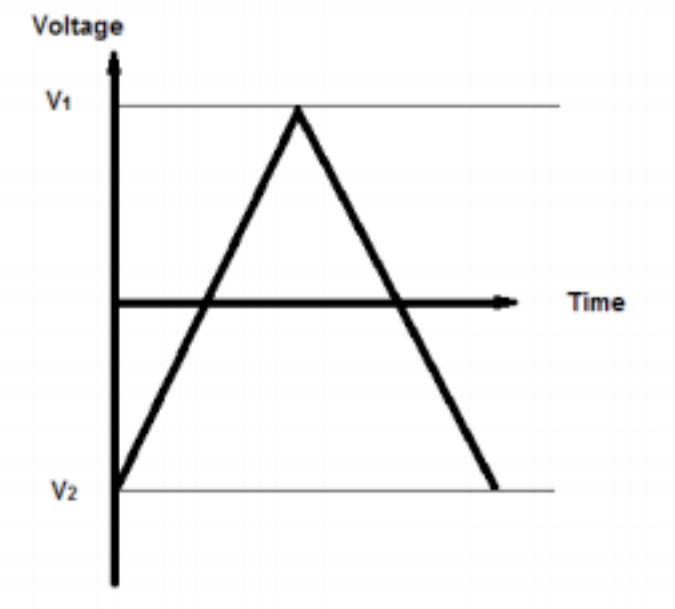

Figure 9: Voltage Sweeps between two voltage limits,V1 and V2 (Gouws, Shawn. 2012)

The current response as a result of this polarization is plotted as a function of the applied potential, which is submitted to cyclic linear scanning between two potential values. The scan rate of the potential can vary over a wide range, but the rate ultimately depends on the projected flow rate of water. This current-voltage curve is referred to as the cyclic voltammogram (Kumpulainen, Heikki et al., 2002). Such a curve is depicted in Figure 10 below:

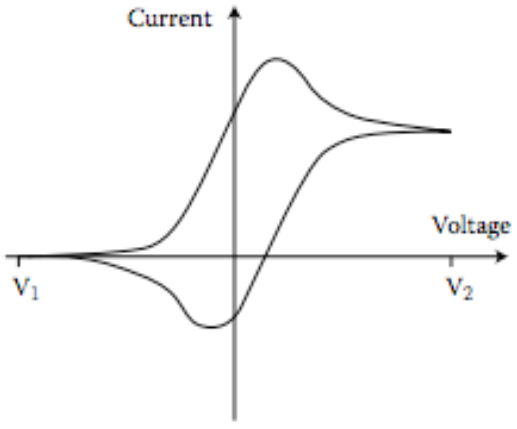

Figure 10: Typical Voltammogram (Wu, Jinfeng et al., 2012)

A cyclic voltammogram can be divided into two regions to represent the oxidation and reduction reactions within the MEA. Region 1, is present from 50-400 mV and represents the oxidation of hydrogen and its transport through the membrane. Region 2, represents the reduction reaction, which occurs between 400-50 mV. At approximately 50 mV molecular hydrogen is formed at the cathode. Figure 11 below illustrates a PEM cyclic voltammogram with specified regions (Cooper, Kevin. 2009).

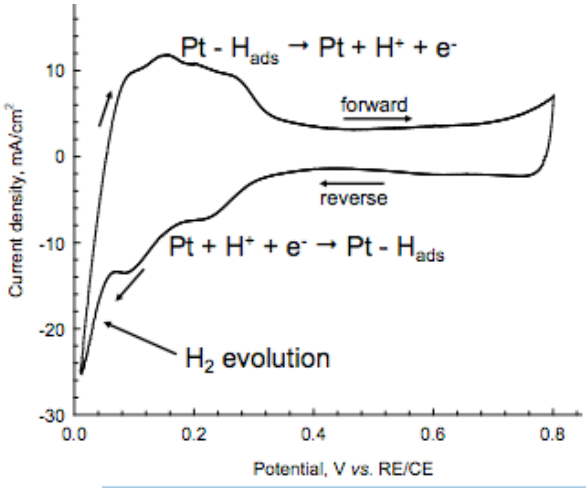

Figure 11: Cyclic voltammogram of PEM fuel cell catalyst (Cooper, Kevin. 2009)

This qualitative information is applied to determine the electrochemical catalyst surface area (ECSA), which an estimate based upon the relationship between the total number of reactive surface sites and the charge needed to remove a monolayer of adsorbed hydrogen on the electrode, as determined from the cyclic voltammetry measurement. The charge is determined by integrating the current density in the cathodic or anodic scan of the hydrogen adsorption/desorption region of the cyclic voltammogram and substituting the capacitive contribution taken between 0.4 V and 0.6 V. The H_2 adsorption charge on a smooth Pt electrode has been measured to be 210 $\frac{\mu C}{cm^2\ Pt}$ of Pt loading in the catalyst layer. The ECSA is calculated using the following equation (Wu, Jinfeng et al.,2012):

$$ECSA\left(\frac{cm^2\,Pt}{g\,Pt}\right) = \frac{Charge\,(\frac{\mu C}{cm^2})}{210\left(\frac{\mu C}{cm^2\,Pt}\right) * Catalyst\ Loading\,(\frac{gPt}{cm^2})} \quad (11)$$

Linear Sweep Voltammetry

Linear sweep voltammetry (LSV) is an electrochemical method to estimate gas crossover through the membrane in a PEM fuel cell. More generally, LSV consists of measuring the current variation when the potential is submitted to a slow scan rate. The information derived from an LSV scan is a useful method to determine fuel cell membrane degradation over a period of time.

During an LSV scan, fully humidified hydrogen is fed to the cathode while an inert gas is fed to the anode. The anode serves as the reference electrode (RE) as well as the counter electrode (CE). The cathode serves as the working electrode (WE). Using a power supply, the WE is swept by a linear potential scan from the initial potential to the final potential at a low scan rate, typically 4 $\frac{mV}{s}$. Commonly, potentials range from 0 V to .5 V. Any potential higher than .8 V is avoided to prevent irreversible platinum or carbon oxidation. Figure 12 below demonstrates a typical LSV curve obtained in the lab.

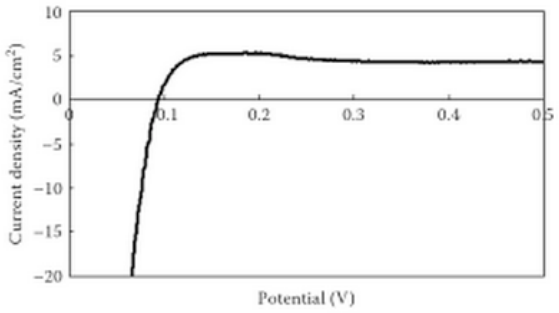

Figure 12: Typical LSV curve measured at 60°C for a commercial Nafion membrane under 100% humidity (Wu, Jinfeng et al., 2012)

When the applied potential of the fuel cell is controlled there is electrochemical activity occurring in the form of current, which is monitored through both the electrodes. Under the chosen high potential, hydrogen has crossed though the membrane from the anode to the cathode. Nitrogen or another inert gas is introduced in the cathode, so any current generated is assumed to correspond to electrochemical oxidation of hydrogen gas that has crossed over from the anode to the cathode, which allows for the estimate of hydrogen crossover from the anode to the cathode. At 0.4 V, hydrogen oxidation occurs and the crossover currant is observed. This current when applied to Faraday's Law, Equation 12, can determine the flow of hydrogen at crossover, thus determining the permeability of the membrane (Zhang, Shengsheng et al., 2012).

$$Q_V = \frac{i_{H_2}}{2F} \qquad (12)$$

Prospective applications

Fuel cells are currently one of the most promising alternative sources of electric power. Fuel cells have a capacity to revolutionize the power industry through offering a cleaner, more-efficient alternative to the combustion of gasoline and other fossil fuels. Fuel cells have the potential to replace internal-combustion engine in vehicles and provide power in both stationary and portable applications because they are energy-efficient, clean, and fuel-flexible (Fuel Cell Technologies Office, DOE). PEM fuel cells are a potential alternative for both automobiles and mobile applications due to their high power density and low temperature operation. In addition, a PEMFC is lightweight, compact and relatively inexpensive to manufacture due to researchers finding new ways to cut costs without sacrificing performance. (Rael, Fox).

A major limitation in fuel cell development and commercialization is the limited lifetime. Depending on the fuel cells applications, the lifetime of a fuel cell stack varies from 2,000 to 10,000 hours, which is still considered insufficient (Lapicque, 2015).

Another major disadvantage of a PEMFC is a delayed voltage supply due to reactant gas flow limitations. A possible solution to this problem is coupling a fuel cell with a battery or supercapacitor. Figure 13 below represents a fuel cell coupled with a capacitor to allow for low voltage operation, which was utilized throughout the duration of this experiment.

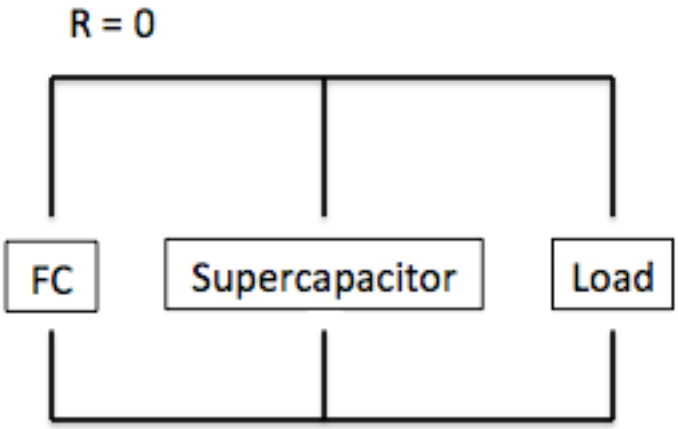

Figure 13: Schematic of fuel cell coupled with a supercapacitor

The fuel cell serves as a current source to charge the supercapacitor or battery. The superconducting coil or supercapacitor would provide zero resistance, thus reducing the fuel cell voltage to approximately zero. The combination of a fuel cell with a battery or supercapacitor is an attractive possibility especially in the automotive industry.

In several previous experiments, PEMFCs were forced to operate at low voltage via CA testing and also via a superconducting coil. Both experiments determined that fuel cells could produce a sufficient current while operating at low voltage. In addition, it was

found that the expected current was correlated to the inlet hydrogen flow rate, thus following Faraday's Law.

This report explored the effects of membrane degradation when a fuel cell is operating in short-circuit. Previous experiments determined that fuel cells were able to provide a current at a low voltage, but the effects of low voltage operation on the fuel cell membrane has yet to be determined. This research intended to determine the effects within the MEA of fuel cell operation coupled with a superconducting coil.

Methodology

Equipment

Fuel Cell

The single PEM fuel cell consists of two end plates, two current collecting plates, two channel flow plates, a bipolar flow plate and a MEA. The MEA consists of a five-layer assembly. The membrane used was a pMembrain H400 (Umicore) purchased from UBzM Germany. On either side of the MEA, were two thin electrodes containing 0.4 mg of platinum per square centimeter, a carbon layer, and two Sigracet® 30BC GDLs. Figure 14 on the following page illustrates the bench setup for the duration of this experiment.

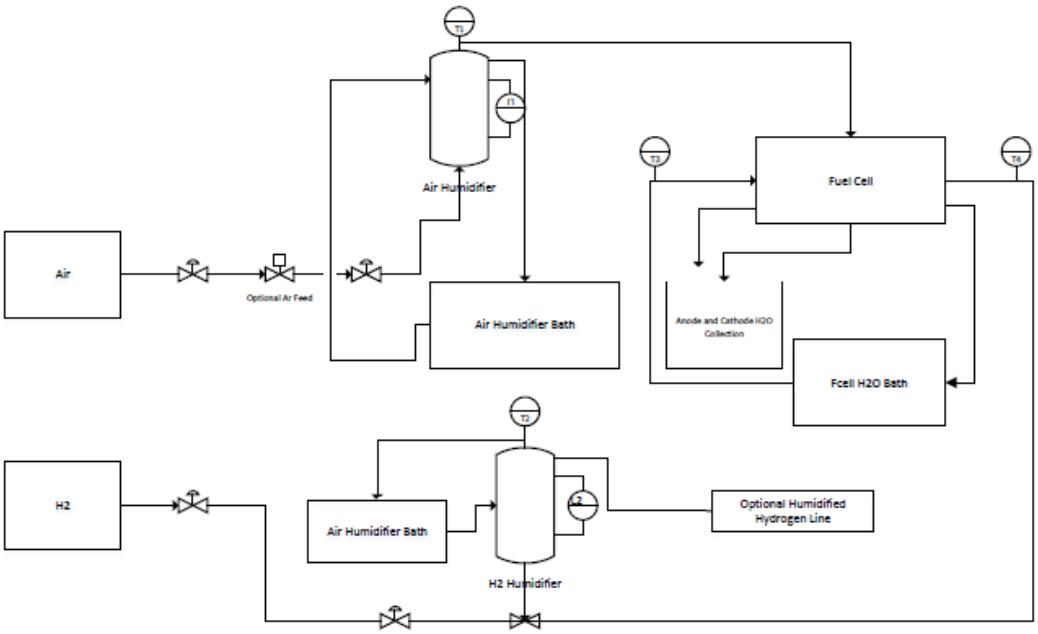

Figure 14: Schematic of fuel cell bench

Air and hydrogen enter the cell from the house supply via valves and regulators. A three-way valve is located downstream of the airflow pathway to allow for argon flow during voltammetry testing. All flow rates are controlled using Brooks® mass flow controllers. Air flows from the house supply into the air humidifier via insulated tubes. The house-made humidifier is connected to a water bath to humidify the air. Once humidified, the air enters the fuel cell at the cathode. For all operations, the hydrogen gas was kept dry and entered the fuel cell at the anode. The fuel cell temperature was maintained at 55°C using preheated water in the cell's water circulation system. Water was collected and recycled from the anode and cathode using a beaker. Figure 15 on the following page is a photo of the actual fuel cell bench.

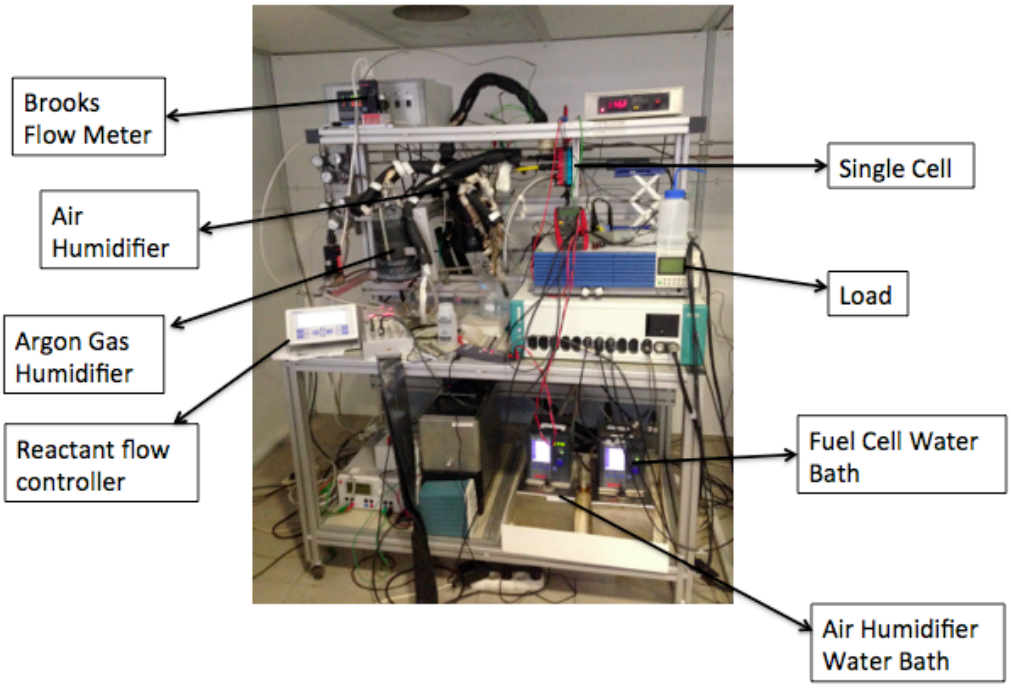

Figure 15: Actual Fuel Cell test bench

On the right of the fuel cell bench is the load and below the load is the potentiostat/galvanostat (PGSTAT). These two pieces of equipment were used together to obtain the level of current necessary for some of the electrochemical experiments. While in galvanostatic mode the PGSTAT is used to control the current between the cathode and anode in the PEM fuel cell (Metrohm Autolab, 2015). However, the PGSTAT can only provide a signal for current between 1 and 2 amps. Using the load the current can be amplified to higher values necessary for the experiments.

Procedures

Polarization Curve and Electrochemical Impedance Spectroscopy

A steady-state polarization curve and a GEIS scan of electrochemical impedance spectra (Nyquist plot) were generated weekly to assess the state of health of the fuel cell.

The measurements for these graphs were obtained for different fixed values of current ranging from 10 A – 120 A. Flow rates for hydrogen and air were increased each time the current was increased using stoichiometric factors of 1.4 for hydrogen and 2.4 for air. The measurements used to make these graphs were cell voltage, imaginary impedance and real impedance. To obtain the necessary measurements, the desired flowrates were set on the regulator on the fuel cell bench. The desired current value was set in NOVA software. However, the desired current value had to be negated when input into the software. The amplitude of the sinusoidal curves was also set in the NOVA software. The amplitude was set to ten percent of the current value. This has been shown to keep the electrochemical system linear while allowing for sufficient accuracy in measurements (Lapicque, 2015). Measurement recoding for voltages less than 700 mV occurred over a duration of 5 minutes and for voltages greater than 700 mV measurements were taken over 10 minutes. From these measurements cell voltage was plotted versus time and the impedance spectra were plotted on a Nyquist plot.

Cyclic Voltammetry and Linear Sweep Voltammetry

For Cyclic Voltammetry (CV) and Linear Sweep Voltammetry (LSV), the flow of air to the humidifier was closed via a three-way valve allowing for the flow of argon gas into the humidifier. Water bath temperatures were increased to 60°C to allow for 100% relative humidity conditions.

Results

The objective of this experiment was to explore the degradation of a single-cell PEM fuel cell while operating at low voltage. This section compiles the results from the various characterization techniques.

The data obtained from the week of January 20th was disregarded because the data obtained during the week of January 26th indicated more accurate representation of fuel cell performance due to the maturation of the system and membrane conditioning.

Comparison of Expected Current and Measured Current Values

The difference between the expected values of current for corresponding flow rates calculated via Faraday's Law and the measured values of current exhibit a general trend of increasing values of current with an increasing flow rate. This trend is exhibited in Figure 16 below:

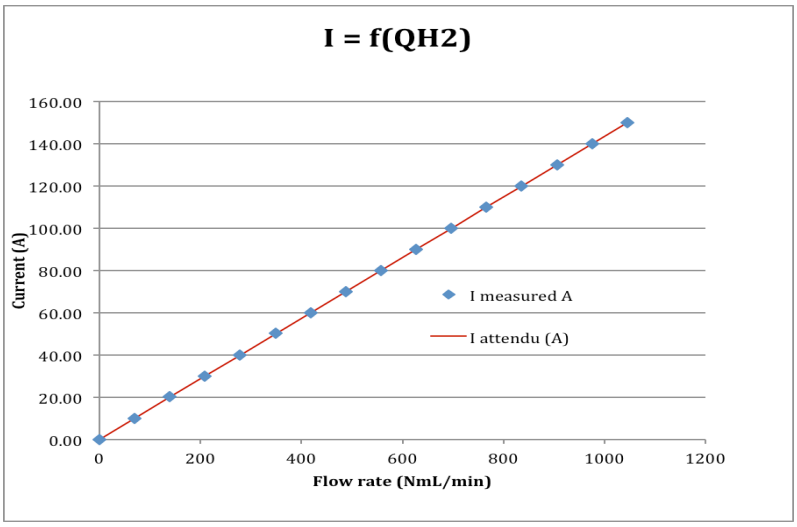

Figure 16: Fuel Cell current as a function of hydrogen flow rate

At higher hydrogen flow rates there was a larger deviation from the general trend of increasing current with increasing flow rate. Specifically for current values of 140A and 150A. See Appendix 3.A. These deviations could be linked to the probe used to take the measurements or the humidification conditions inside the fuel cell.

Figure 17 on the following page shows the short circuit resistance (R_{sc}) or the ratio of measured voltage to measured current for the week of February 2, 2015.

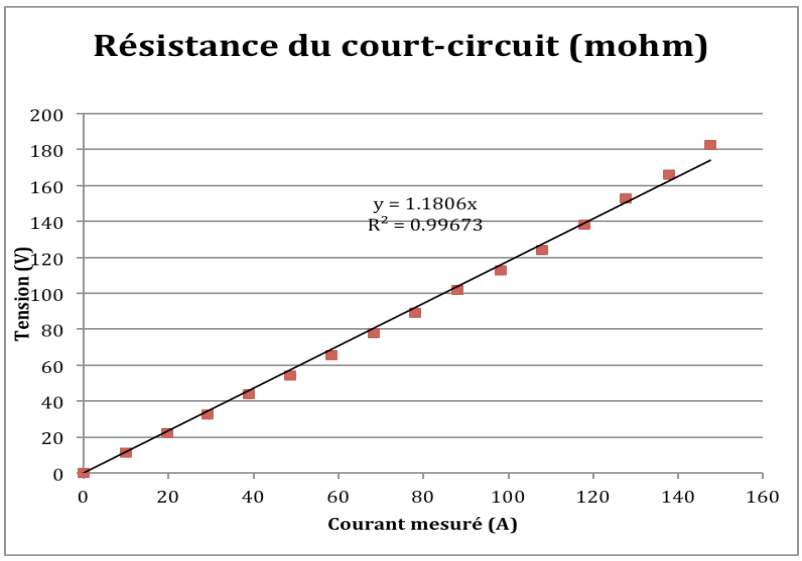

Figure 17: Short-Circuit Resistance for 2-Feb-2015

The resulting short circuit resistance (R_{sc}) is the slope of the line generated by plotting the measured voltage versus the measured current. For the week of February 2, 2015 the R_{sc} is equal to 1.1806. As evidenced in Appendix 3.B, the value of R_{sc} remained fairly constant throughout the six weeks of testing. This relatively constant value of R_{sc} exemplifies that the cell generates constant resistance while operating in short circuit over the course of 6 weeks.

Polarization Curves

It was found that the voltage decreases with increasing current density. The rate at which the voltage decreased became greater as the weeks progressed. At low current densities between .1 and .3 A/cm^2 the deviation in the voltage between the different weeks was not as large as it was at high current densities between .4 and 1.3 A/cm^2. The polarization curves containing results for each week are shown in Figure 18.

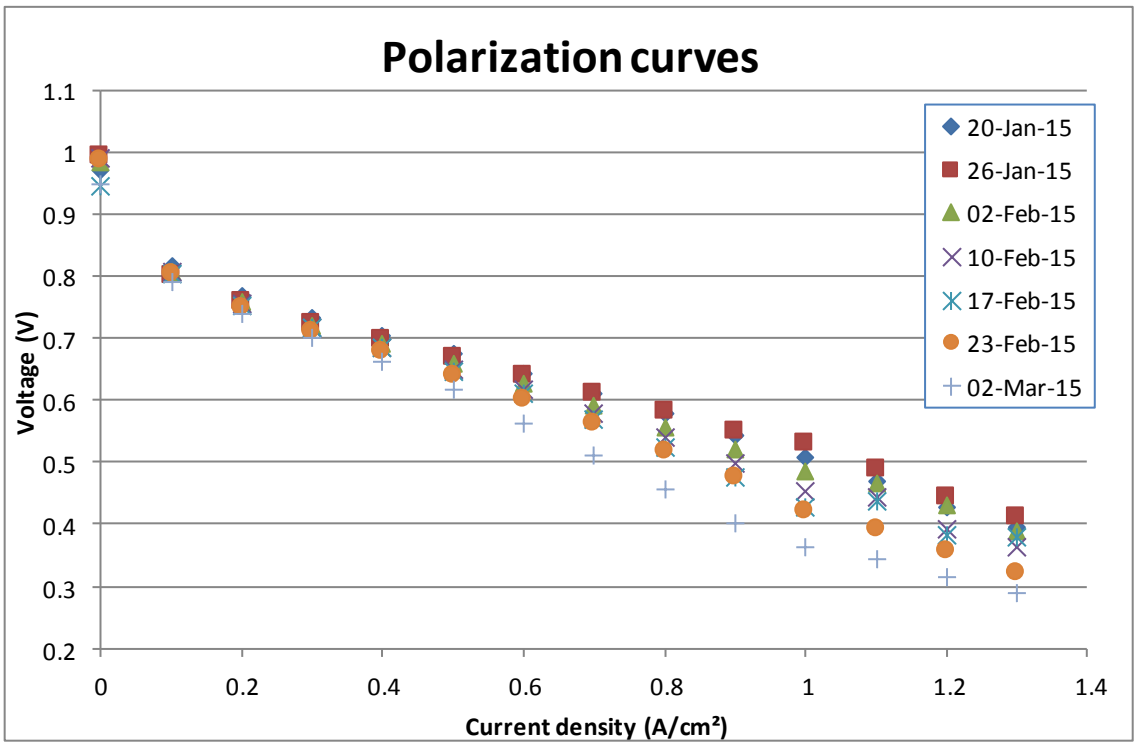

Figure 18: Polarization Curves for PEM Fuel Cell at 55°C

Performance Curve

From the polarization curve data the performance curve of power density (P_d) versus current density was plotted. As can be seen in Figure 19 below:

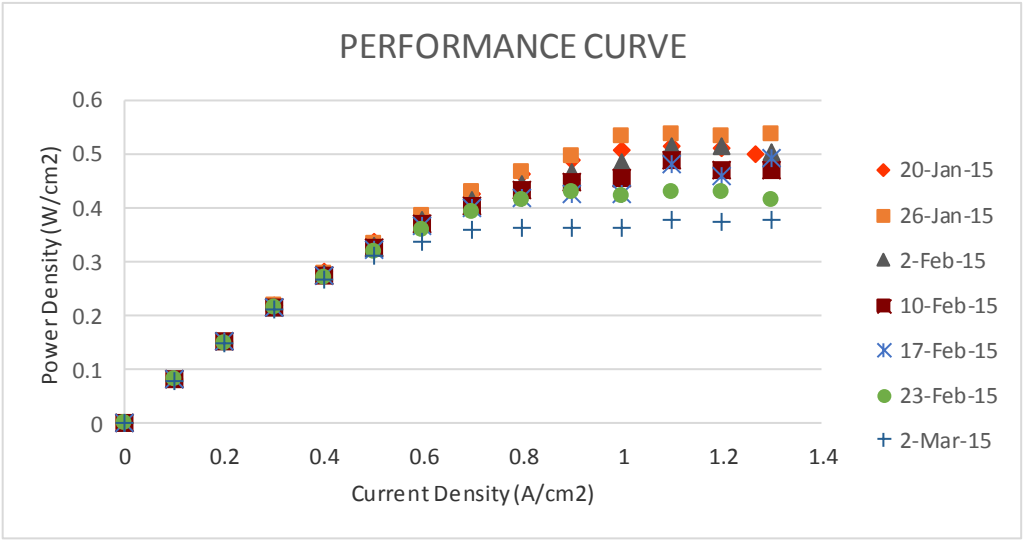

Figure 19: Performance decreased over the course of the 6 weeks

Electrochemical Impedance Spectroscopy

The ohmic resistance values are shown in Figure 20, below, as a function of time. Ohmic resistance fluctuated greatly initially but as time increased the ohmic resistance began to increase as can be seen on the right half of Figure 20. This increase in ohmic resistance with time indicates decreased conductivity in the fuel cell. The initial decrease in ohmic resistance may be related to the level of humidity in the cell and the conditions under which the cell was conditioned. An over-humidified or under-humidified MEA may not be an environment conducive to maximum conductivity.

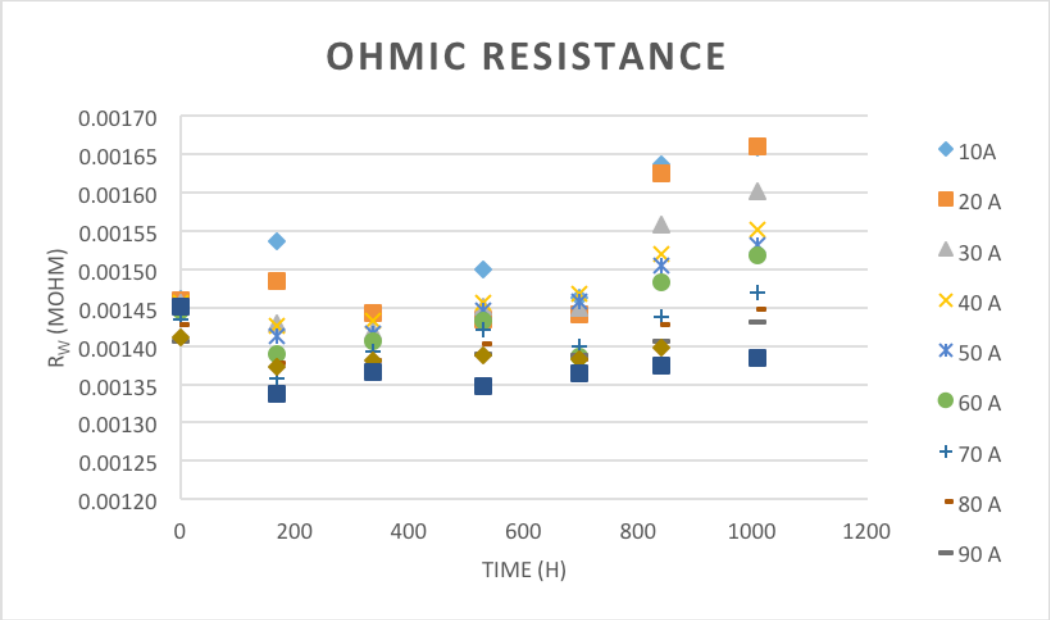

Figure 20: Values for ohmic resistance as determine by fitting EIS data to a model Values for charge transfer resistance were obtained in addition to those for ohmic

resistance. Both values of charge transfer resistance at the cathode (R_c) and charge transfer resistance at the anode (R_a) were obtained. R_c is plotted as a function of time in Figure 21 on the following page. R_c remains quite constant for a given value of current as time progresses. This indicates that there is not a significant change in hydrogen reduction at the cathode.

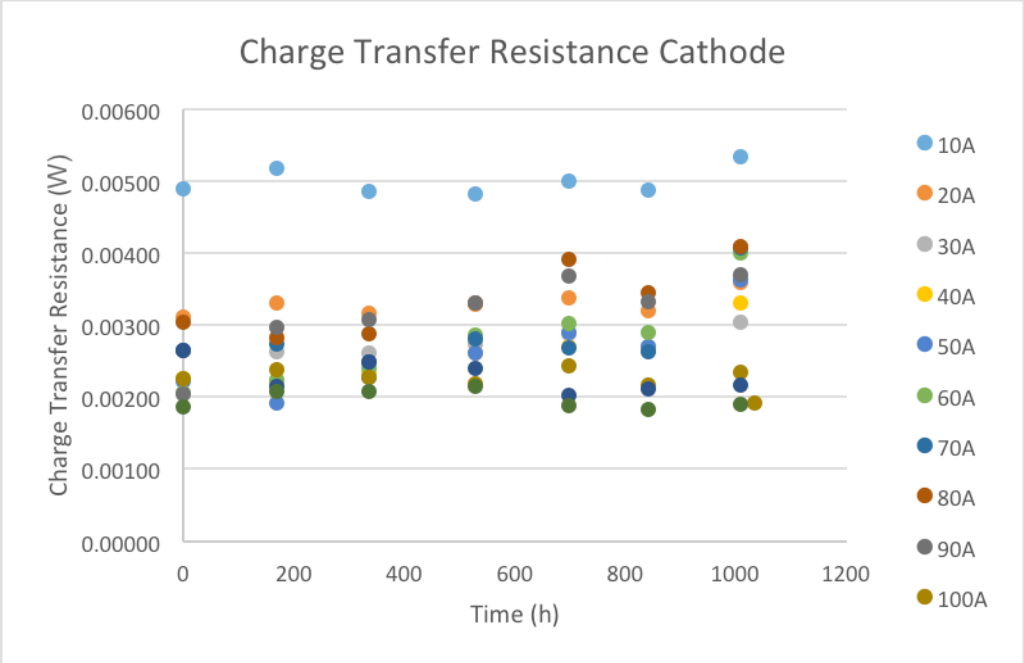

Figure 21: Values for charge transfer resistance at the cathode.

Results similar to those of R_c are shown for R_a in Figure 22. It was assumed that R_a was ten percent of R_c. Since the values for these resistances are constant the conductufuty of the fuel cell can not be attributed to any changes in fuel cell performance within the time frame of these experiments.

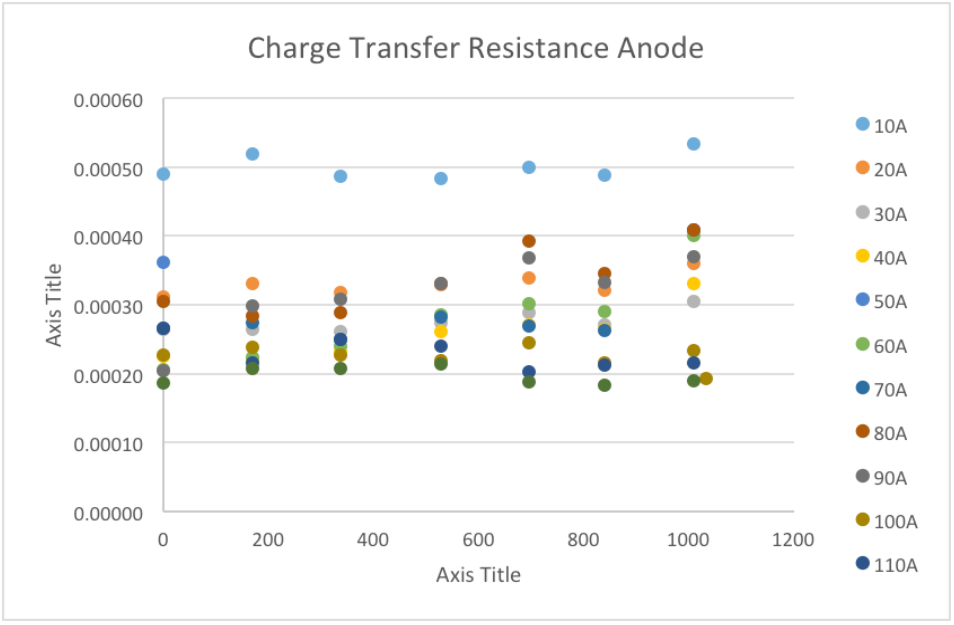

Figure 22: Values for charge transfer resistance at the anode.

The final type of resistance that was determined with EIS was diffusion resistance. As can be seen in Figure 23 below, diffusion resistance increases with time in almost a linear fashion, especially at current levels below 70A. This increase may be attributed to the cell components becoming more compressed an gas flow more difficult, thus hindering mass transfer. Diffusion resistance increases with current as well (greater than 70 A) where there is an average of a 2.4 fold increase in diffusion resistance over the time interval. The average diffusion resistance values are greater at higher levels of current indicating a greater hinderance to mass transfer possibly due to reaching the limiting current $i_{l,}$ at which the resistance to reaction is mainly controlled by diffusion resistance as opposed to charge transfer resistance.

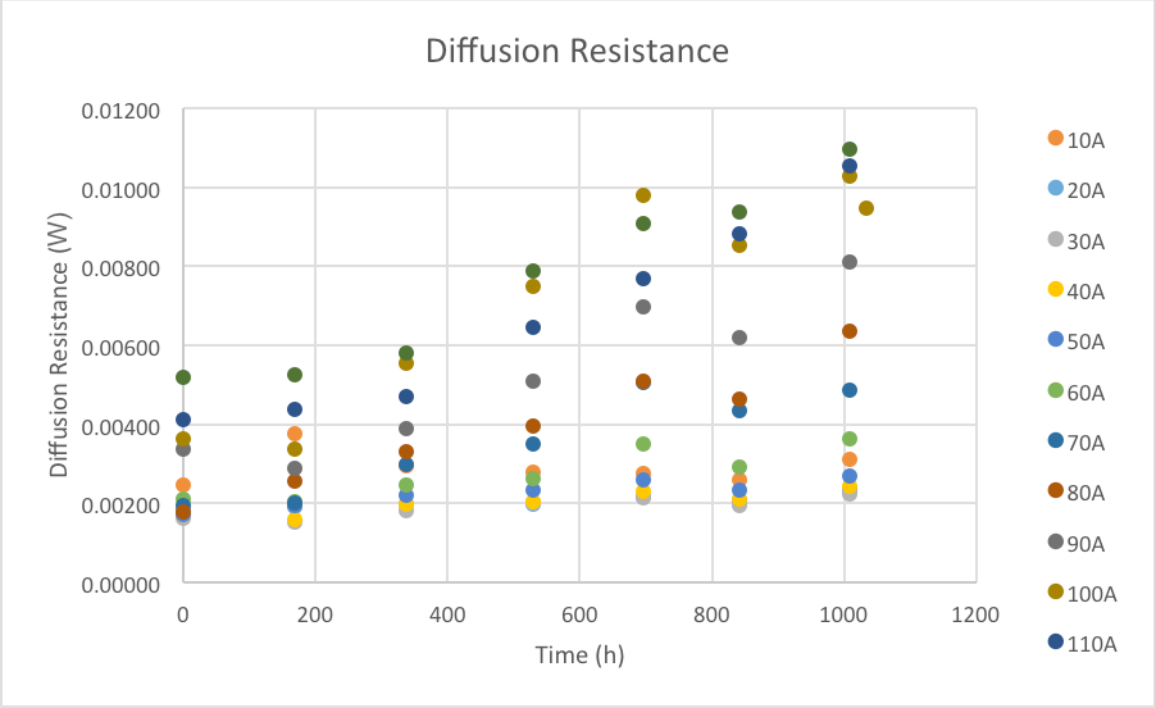

Figure 23: Diffusion resistance values over seven week timeframe.

The pseudocapacitance, which is a double layer capacitance is shown in Figure 24 and Figure 25 at the cathode and the anode. At the cathode the pseudocapacitance

increases and then decreases over time whereas at the anode it reamains fairly constant for values of current below 40 A and for 90 A and 120 A. The variaton in pseudocapacitance is slight, however, so no conclusions can be drawn from the capacitance within the time frame of this experiment.

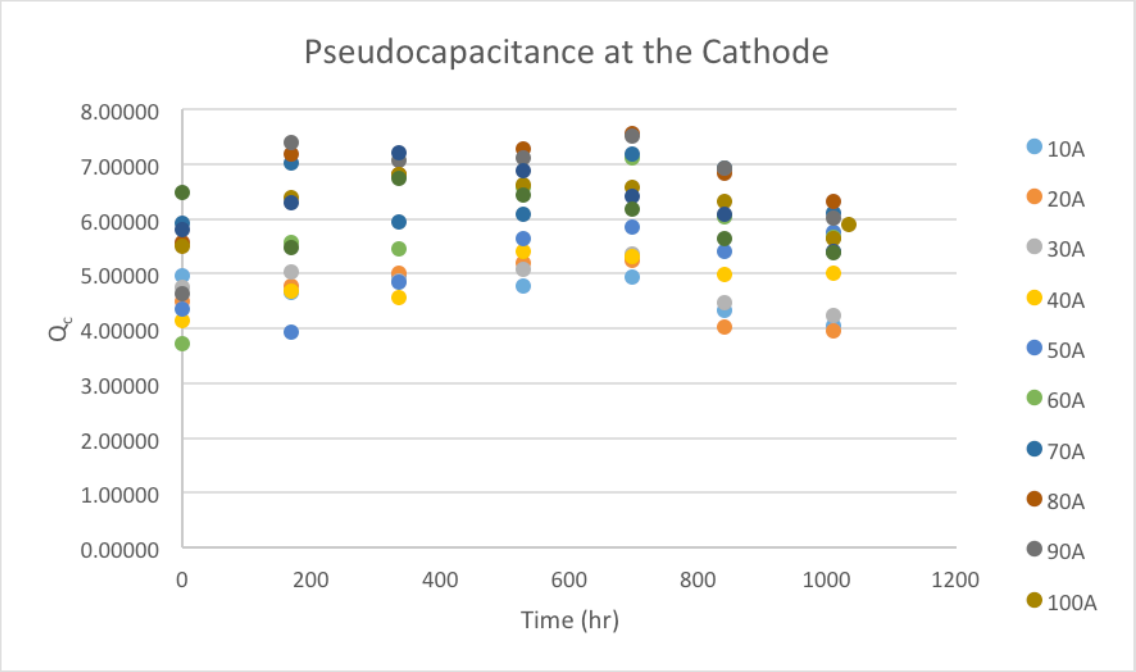

Figure 24: Pseudo capacitance at the cathode

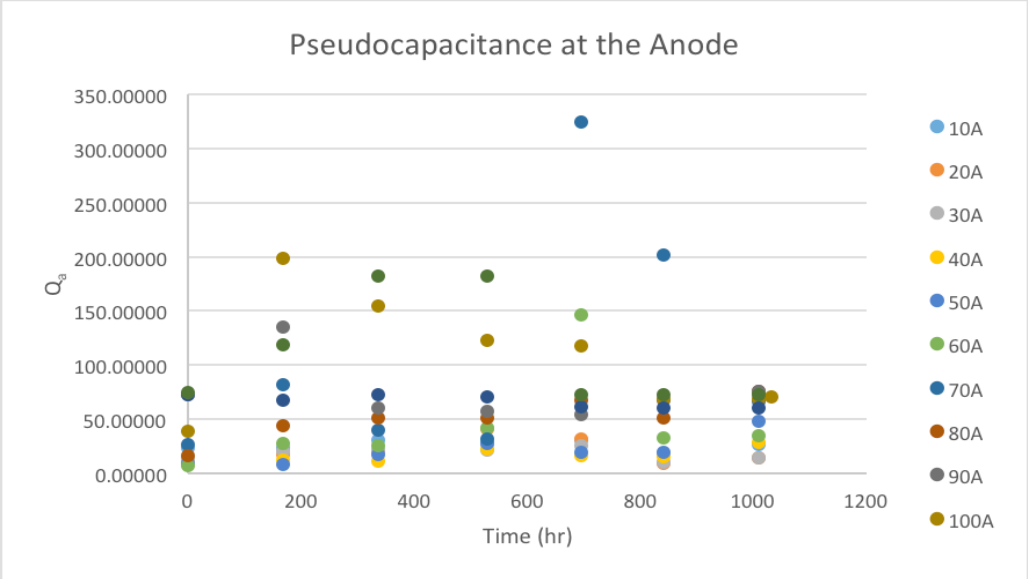

Figure 25: Pseudo capacitance at the anode

Two model parameters used in the equivalent circuit model for the pseudo capacitance calculation do give some insight into the effect of capacitance on the fuel cell indirectly and these are the exponents of charge of constant phase element at the cathode (nc) and at the anode (na). These parameters represent how well the electrode can accommodate pseudo capacitance and are shown in Figure 26 and Figure 27 below:

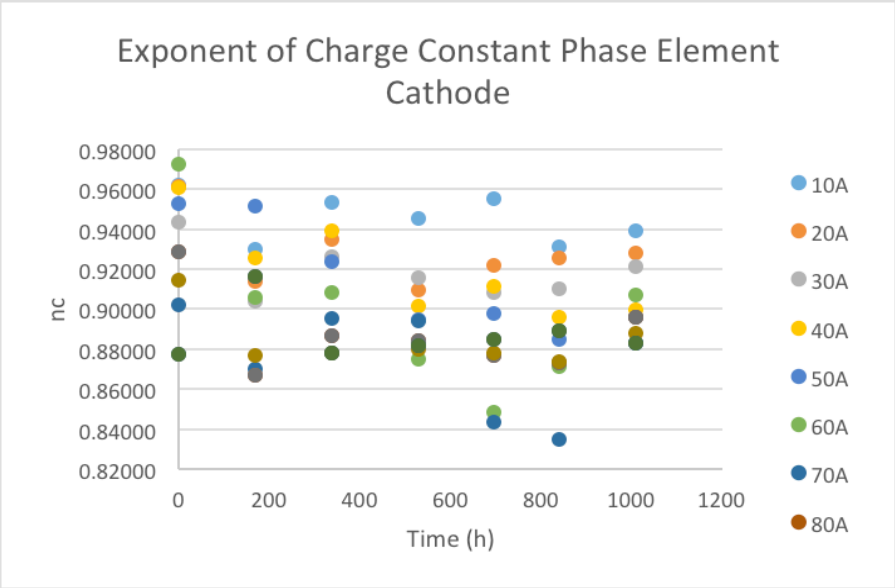

Figure 26: Exponent of charge of constant phase element at the cathode

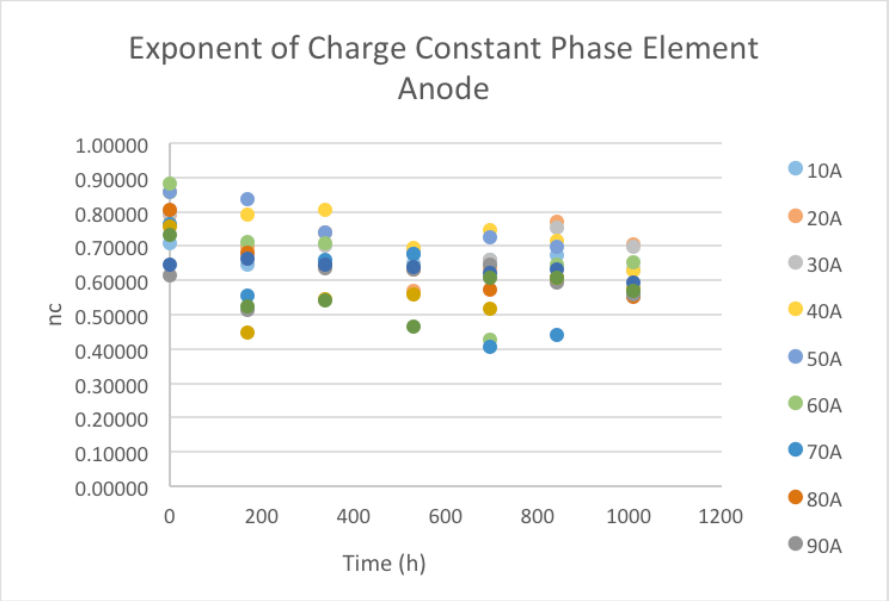

Figure 27: Exponent of charge of constant phase element at the cathode

A low nc of around .5 and .6 means the electrode interface is not well defined. Both nc and na decrease overall overtime and with increasing levels of current even though some fluctuations are present. The exponent for the anode decreases more than the exponent for the cathode as time increases. Nc does not decrease by more than .1 whereas na decreases by values between .1 and .3. The cathode interface is consistently more defined and more stable than the anode interface but overall there is not a significant change in either electrode.

Cyclic Voltammetry and Linear Sweep Voltammetry

Table 2, summarizes the ESCA values obtained via CV testing at a scan rate of 30 mV/s.

Date	20-Jan-15	26-Jan-15	2-Feb-15	10-Feb-15	17-Feb-15	23-Feb-15	2-Mar-15
Time (h)		0	168	360	528	672	840
ECSA in cm^2Pt/cm^2	164.6	137.7	158.7	158.7	131.7	142.8	101.2

Table 2: ECSA values at a scan rate of 30 mV/s

The data obtained from the week of January 20th was disregarded because the value of ESCA is sensitive to the hydration of the membrane. The ESCA value obtained from the data collected on the week of February 17th is slightly lower than what is anticipated. The expected value should be around 140 cm^2Pt/cm^2. This lower ESCA value could be due to a low inlet gas temperature entering the fuel cell.

There were no significant changes in the ESCA value. This suggests that the catalyst suffered little during the aging process while the fuel cell operated at low voltage.

Table 3 on the following page summarizes the hydrogen crossover results obtained from LSV.

Date	20-Jan-15	26-Jan-15	2-Feb-15	10-Feb-15	17-Feb-15	23-Feb-15	2-Mar-15
Time (h)		0	168	360	528	672	840
H2 crossover (mA)	87.0	58.3	100.0	97.0	100.0	100.0	104.0

Table 3 : Hydrogen Crossover over six week period

The value of hydrogen crossover suggests the membrane capacity to be porous or nonporous. The value for hydrogen crossover remains fairly constant, so there was no considerable membrane aging during low voltage operation. These results suggest that there is no membrane degradation, since the permeability is virtually unchanged.

It is suggested to continue running weekly characterization tests for a longer duration of time because the general trend for fuel cell aging is a steady slow decline followed by rapid aging. For both LSV and CV, there were larger changes in ESCA and hydrogen crossover from the week of February 23rd to March 2nd compared to the changes in other weeks. During the final week of testing, the ESCA value suggests greater catalyst degradation than previous weeks. In addition during the final week of testing for LSV, there was a slight decrease in fuel crossover, which suggests an increase in porosity or aging of the membrane.

Conclusions and Recommendations

Characterization of the fuel cell membrane while in short-circuit operation yielded no significant degradation on the health of the fuel cell.

The results from the electrochemical impedance spectroscopy (EIS) and polarization curve results illustrate a decrease in fuel cell performance over the course of this experiment. However, the results obtained during voltammetry testing imply there were no significant changes in the catalyst health and membrane porosity.

These results suggest that there are another phenomena responsible for the fuel cells decrease in performance. The EIS diffusion resistance results suggest that there was an increasing mass transport limitation over the course of the experiment. The mass transport limitation could be due to the degradation of the electrodes and/or GDLs. The fuel cell is assembled tightly, so this compression over a long period of time could result in the degradation of other parts of the fuel cell, which would result in a decrease in performance.

Characterization of the fuel cell yielded very comparable results from the MQP project completed by Veronica Goldsmith and Lindsey Mitchel last year titled *Effects of Low Voltage Testing on PEM Fuel Cell with Current Control by Hydrogen Flow*. Their experimentation proved the validity of Faraday's law by controlling the current density through the flow of hydrogen feed. In addition, their results suggested that there was minimal MEA damage caused by low voltage operation over a long duration of time.

Overall, the experimental results from both this report and last years report suggest that conjunction of a fuel cell with a supercapacitor is an attractive application. Since, the current density is controlled by hydrogen flow this allows for a simple efficient process that is easily controllable. In addition, the ability to couple a fuel cell with a supercapacitor allows the cell to charge the supercapacitor, which decreases the reactant flow rate limitation thus controlling the power output.

It is recommended to continue the four weekly characterization tests on the fuel cell until the membrane dies. Over the course of the six weeks, the membrane showed insignificant degradation. However, the typical aging of a fuel cell is a slow plateau followed by a rapid decline in health. It is also recommended to investigate the effect of short circuit operation on a fuel cell stack. This experiment focused on a single stack.

However in order to apply fuel cells to power a given application multiple cell stacks are typically needed.

In future experiments, it would be beneficial to also conduct weekly tests to monitor of the health of the electrodes and GDLs to determine if these fuel cell components are adversely effected by short-circuit operation.

Overall, this research provides information of the long-term health of a single MEA operating at low voltage. It is important to analyze and understand the factors that hinder fuel cell technology in order to continue making improvements.

Appendix I: Reactant flow rate calculations

Using a form of Faraday's Law, $= \frac{I}{2*F} * \frac{RT}{p}$, flowrates at various currents were calculated. The following oxidation reduction reactions taking place in the fuel cell were also considered in these calculations.

$$2H_2 \rightarrow 4H^+ + 4e^-$$

$$O_2 + 4H^+ + 4e^- \rightarrow 2H_2O$$

Flowrate of Hydrogen

If I = 10 A, $Q_{H2} = \frac{I}{2*F}\frac{mol}{s} * \frac{8.314*273}{101325}\frac{L}{mol} * 1000\frac{ml}{L} * \frac{60\ s}{min} = 69.65\ \frac{ml}{min}$ at STP,

where 2 is the number of electrons involved in hydrogen oxidation,

F = 96485 $\frac{C}{mol}$, R = 8.314 $\frac{J}{mol\ K}$

and $\frac{R*T}{p} = molar\ volume$ from the Ideal Gas Law: $\frac{p}{V} = nRT$.

To obtain the actual flowrate of hydrogen the 69.65 $\frac{ml}{min}$ was multiplied by a correction factor, **I**=1.4. This ensured a forty percent excess of hydrogen.

$Q_{H2actual} = 69.65\frac{ml}{min} * 1.4 = 97.51\frac{ml}{min}$.

Flowrate of Oxygen

If I = 10 A ,$Q_{O2} = \frac{I}{4*F}\frac{mol}{s} * \frac{8.314*273}{101325}\frac{L}{mol} * 1000\frac{ml}{L} * \frac{60\ s}{min} = 34.82\ \frac{ml}{min}$ at STP,

where 4 is the number of electrons involved in oxygen reduction,

F = 96485 $\frac{C}{mol}$, R = 8.314 $\frac{J}{mol\ K}$

and $\frac{R*T}{p} = molar\ volume$ from the Ideal Gas Law: $\frac{p}{V} = nRT$.

$$Q_{air} = \frac{Q_{O2}}{.21} = \frac{34.82}{.21} = 165.83\ \frac{ml}{min}$$

To obtain the actual flowrate of air 165.83 $\frac{ml}{min}$ was multiplied by a correction factor, **l**=2.4. This correction factor corresponds to a one hundred forty percent excess of oxygen in air.

$$Q_{air\ actual} = \frac{Q_{O2}}{.21} = 165.83\frac{ml}{min} * 2.4 = 398\ \frac{ml}{min}$$

Calculations yielded Table 4 on the following page:

I (A)	**Q_{H2} (NmL/min) 1.4**	**Q_{air} (NmL/min) 2.4**
0	0	0
10	97.51	397.98
20	195.01	795.96
30	292.52	1193.94
40	390.02	1591.92
50	487.53	1989.91
60	585.03	2387.89
70	682.54	2785.87
80	780.04	3183.85
90	877.55	3581.83
100	975.05	3979.81
110	1072.56	4377.79
120	1170.06	4775.77
130	1267.57	5173.75

Table 4: Flow rates for hydrogen and air calculated with Faraday's Law

Appendix II: Calibration of Flow Meters

Before starting the experiments the hydrogen and air flow meters were calibrated. The appropriate calibration unit (different calibration units had different max flows that they could handle) was hooked up to the flowmeter being calibrated. The regulator was set to the desired flowrate "set point". An average of ten readings, shown on the regulator screen, for the flowrate was recorded. This was repeated for twelve "set points" ranging from minimum to maximum flowrates for each calibration unit. The maximum flow rate for a particular calibration unit was indicated on the calibration unit and the minimum flow rate was the maximum divided by fifty. The average flow rates obtained were graphed versus the desired flow rate "set points" and the correction factor for the flow meter was taken as the equation of the resulting line. An example correction factor is shown in Figure 28 below:

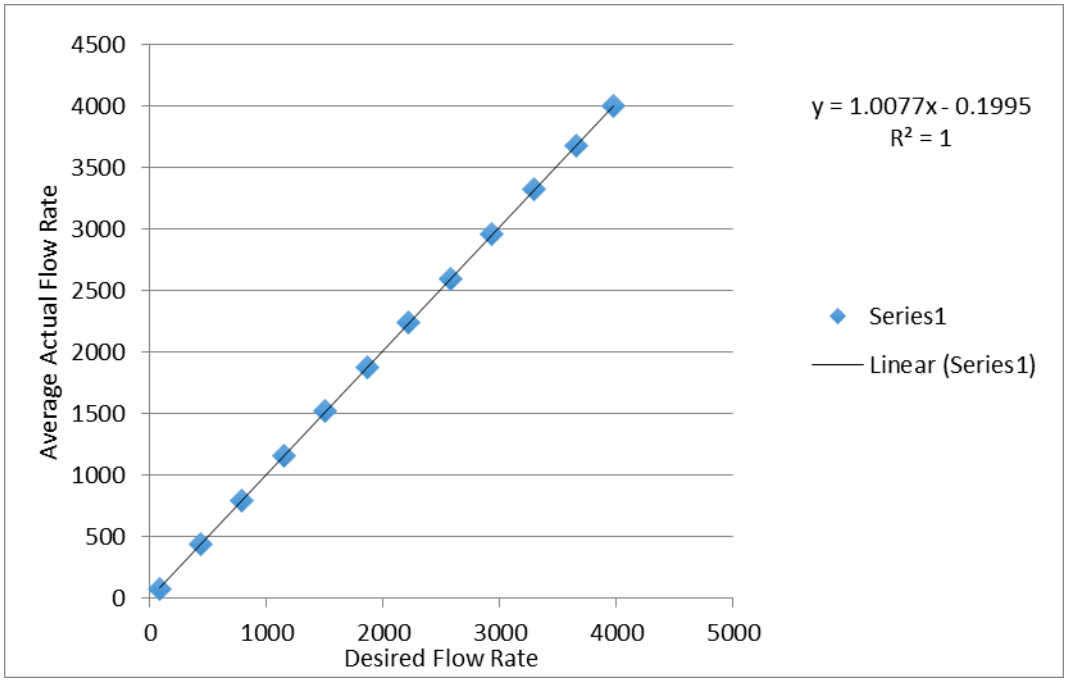

Figure 28: Average Actual Flow Rate versus Desired Flow Rate

Appendix III: Raw Data

A. Expected Current and Measured Current Value

		20-Jan-15			26-Jan-15		
Q(H2)	**I expected**	**I measured**	**I difference**	**U**	**I measured**	**I difference**	**U**
NmL/min	**A**	**A**	**A**	**mV**	**A**	**A**	**mV**
0	0.00	not done			0	0.00	0
70	10.05				9.95	0.10	13.9
140	20.10				19.7	0.40	27.2
209	30.01				29.3	0.71	40.2
279	40.06				39.1	0.96	53.5
349	50.11				48.9	1.21	66.9
418	60.02				58.6	1.42	80.3
488	70.07				68.6	1.47	94.6
558	80.12				78.5	1.62	108.8
627	90.03				88.3	1.73	123.5
697	100.08				98.3	1.78	138.5
766	109.98				108.2	1.78	152.4
836	120.03				118	2.03	170.1
906	130.09				128	2.09	187.8
976	140.14				138	2.14	205.7
1045	150.04				147.5	2.54	224.5
					Rsc	1.44	mohm

		2-Feb-15			10-Feb-15		
Q(H2)	**I expected**	**I measured**	**I difference**	**U**	**I measured**	**I difference**	**U**
NmL/min	**A**	**A**	**A**	**mV**	**A**	**A**	**mV**
0	0.00	0	0.00	0	0.0	0.0	0.0
70	10.05	9.95	0.10	11.3	10.0	0.1	11.0
140	20.10	19.7	0.40	22.1	19.7	0.4	21.4
209	30.01	29.3	0.71	32.7	29.3	0.7	31.6
279	40.06	39.1	0.96	43.7	39.1	1.0	42.2
349	50.11	48.8	1.31	54.4	48.7	1.4	52.5
418	60.02	58.4	1.62	65.7	58.4	1.6	63.2
488	70.07	68.4	1.67	77.7	68.3	1.8	74.3
558	80.12	78.2	1.92	89.3	78.1	2.0	85.6
627	90.03	88	2.03	102.1	88.1	1.9	98.0
697	100.08	98.2	1.88	112.6	98.1	2.0	110.0
766	109.98	107.9	2.08	124.1	107.7	2.3	117.8
836	120.03	117.9	2.13	138.4	117.8	2.2	132.1
906	130.09	127.8	2.29	152.9	127.7	2.4	146.0
976	140.14	138	2.14	165.9	137.7	2.4	161.0
1045	150.04	147.6	2.44	182.6	147.3	2.7	177.0
		Rsc	1.18	mohm	Rsc	1.14	mohm

		17-Feb-15			23-Feb-15		
Q(H2)	**I expected**	**I measured**	**I difference**	**U**	**I measured**	**I difference**	**U**
NmL/min	**A**	**A**	**A**	**mV**	**A**	**A**	**mV**
0	0.00	0	0.00	0	0	0.00	0
70	10.05	10	0.05	14	10.05	0.00	12.2
140	20.10	19.9	0.20	27.5	20.1	0.00	23.5
209	30.01	29.4	0.61	40.7	29.85	0.16	35.2
279	40.06	39.35	0.71	54.4	39.75	0.31	47
349	50.11	49.05	1.06	67.8	49.35	0.76	58.7
418	60.02	59	1.02	82	59.35	0.67	70.9
488	70.07	69.1	0.97	97.2	69.35	0.72	83.5
558	80.12	79.1	1.02	112	79.35	0.77	95.9
627	90.03	89.2	0.83	127.2	89.35	0.68	109.4
697	100.08	98.8	1.28	143	99.4	0.68	122.7
766	109.98	108.5	1.48	150	109.2	0.78	135.7
836	120.03	118.2	1.83	172	119.2	0.83	151
906	130.09	127.7	2.39	193	129.2	0.89	166.9
976	140.14	135.5	4.64	207	139.3	0.84	183.5
1045	150.04	141.3	8.74	220	147.35	2.69	198.8
		Rsc	1.47	mohm	Rsc	1.27	mohm

		2-Mar-15		
Q(H2)	**I expected**	**I measured**	**I difference**	**U**
NmL/min	**A**	**A**	**A**	**mV**
0	0.00	0	0.00	0
70	10.05	10.6	-0.55	11.8
140	20.10	20.4	-0.30	22.8
209	30.01	30.3	-0.29	34.1
279	40.06	40.3	-0.24	45.6
349	50.11	49.9	0.21	56.8
418	60.02	59.8	0.22	68.6
488	70.07	70	0.07	80.7
558	80.12	79.8	0.32	92.5
627	90.03	90	0.03	105
697	100.08	100	0.08	117.5
766	109.98	110	-0.02	130.9
836	120.03	120.2	-0.17	144.1
906	130.09	130.1	-0.01	157.7
976	140.14	136.1	4.04	169
1045	150.04	139.5	10.54	176
		Rsc	1.2	mohm

B. Polarization Curves

	20-Jan-15	26-Jan-15	2-Feb-15	10-Feb-15	17-Feb-15	23-Feb-15	2-Mar-15	
i (A/cm²)	**U (V)**	**U (V)**	**U (V)**	**U (V)**	**U (V)**	**U (V)**	**U (V)**	
0	0.973	0.995	0.985	0.992	0.947	0.988	0.95	
0.1	0.816	0.8	0.807	0.806	0.803	0.803	0.79	
0.2	0.768	0.758	0.758	0.757	0.754	0.75	0.739	
0.3	0.733	0.725	0.722	0.717	0.718	0.712	0.701	
0.4	0.703	0.698	0.691	0.686	0.686	0.677	0.664	
0.5	0.674	0.67	0.66	0.651	0.648	0.641	0.619	
0.6	0.644	0.641	0.628	0.617	0.611	0.602	0.563	
0.7	0.611	0.612	0.593	0.579	0.569	0.562	0.512	
0.8	0.578	0.583	0.557	0.54	0.524	0.518	0.456	
0.9	0.543	0.55	0.52	0.499	0.475	0.477	0.402	March 3rd
1	0.508	0.532	0.484	0.454	0.427	0.422	0.362	0.394
1.1	0.468	0.489	0.4667	0.443	0.438	0.391	0.344	
1.2	0.426	0.444	0.43	0.392	0.383	0.357	0.313	
1.3	0.394	0.412	0.388	0.362	0.378	0.32	0.29	

C.EIS

10A														
				CATHODE					ANODE					
	Time	L	Rohm	Rc	Qc	nc	Rd c	Td c	Ra	Qa	na	(Rct + Rd)	% Rct	%Rd
	h	H	ohm	ohm	ad^(1-n).s^(n-1)		ohm	s	ohm	ad^(1-n).s^(n-1)				
20-Jan-15	0	2.40E-08	0.00146	0.00490	4.96853	0.96228	0.00246	0.39077	0.00049	24.08694	0.70882	0.00785	68.6%	31.4%
26-Jan-15	168	2.60E-08	0.00154	0.00518	4.65919	0.92995	0.00375	0.52633	0.00052	23.38410	0.64517	0.00945	60.3%	39.7%
2-Feb-15	336	2.60E-08	0.00144	0.00487	4.95329	0.95329	0.00295	0.43527	0.00049	31.22270	0.65570	0.00830	64.5%	35.5%
10-Feb-15	528	2.60E-08	0.00150	0.00483	4.77245	0.94548	0.00278	0.36871	0.00048	27.95784	0.64902	0.00809	65.6%	34.4%
17-Feb-15	696	2.00E-08	0.00146	0.00500	4.94605	0.95531	0.00274	0.36492	0.00050	31.03952	0.65959	0.00823	66.7%	33.3%
23-Feb-15	840	2.00E-08	0.00164	0.00488	4.33913	0.93131	0.00257	0.34447	0.00049	18.84137	0.67475	0.00794	67.6%	32.4%
2-Mar-15	1008	2.10E-08	0.00166	0.00534	4.04040	0.93927	0.00312	0.34977	0.00053	26.33229	0.63096	0.00900	65.3%	34.7%

20A														
				CATHODE					ANODE					
	Time	L	Rohm	Rc	Qc	nc	Rd c	Td c	Ra	Qa	na	(Rct + Rd)	% Rct	%Rd
	h	H	ohm	ohm	ad^(1-n).s^(n-1)		ohm	s	ohm	ad^(1-n).s^(n-1)				
20-Jan-15	0	2.40E-08	0.00146	0.00312	4.49248	0.96154	0.00182	0.19758	0.00031	13.07901	0.79063	0.00525	65.3%	34.7%
26-Jan-15	168	2.60E-08	0.00148	0.00330	4.77961	0.91365	0.00189	0.21899	0.00033	17.05966	0.69720	0.00552	65.7%	34.3%
2-Feb-15	336	2.50E-08	0.00144	0.00317	5.01605	0.93516	0.00197	0.19057	0.00032	19.37504	0.73990	0.00546	63.9%	36.1%
10-Feb-15	528	2.70E-08	0.00143	0.00330	5.20471	0.90961	0.00196	0.18944	0.00033	40.77832	0.56976	0.00559	64.9%	35.1%
17-Feb-15	696	2.10E-08	0.00144	0.00338	5.24791	0.92217	0.00218	0.19167	0.00034	31.84271	0.63442	0.00590	63.1%	36.9%
23-Feb-15	840	2.00E-08	0.00162	0.00320	4.02193	0.92575	0.00207	0.17666	0.00032	9.03538	0.76913	0.00560	63.0%	37.0%
2-Mar-15	1008	2.10E-08	0.00166	0.00360	3.94872	0.92786	0.00232	0.15777	0.00036	14.05173	0.70650	0.00628	63.0%	37.0%

30A														
				CATHODE					ANODE					
	Time	L	Rohm	Rc	Qc	nc	Rd c	Td c	Ra	Qa	na	(Rct + Rd)	% Rct	%Rd
	h	H	ohm	ohm	ad^(1-n).s^(n-1)		ohm	s	ohm	ad^(1-n).s^(n-1)				
20-Jan-15	0	2.40E-08	0.00146	0.00264	4.74378	0.94385	0.00162	0.13329	0.00026	13.86828	0.79602	0.00452	64.3%	35.7%
26-Jan-15	168	2.60E-08	0.00143	0.00263	5.03303	0.90419	0.00152	0.12573	0.00026	20.95858	0.67782	0.00442	65.6%	34.4%
2-Feb-15	336	2.60E-08	0.00142	0.00261	4.87519	0.92652	0.00182	0.12560	0.00026	21.60795	0.70132	0.00468	61.2%	38.8%
10-Feb-15	528	2.60E-08	0.00145	0.00275	5.08344	0.91547	0.00201	0.12774	0.00027	21.12684	0.69018	0.00503	60.0%	40.0%
17-Feb-15	696	2.10E-08	0.00145	0.00289	5.34938	0.90838	0.00212	0.12769	0.00029	25.60207	0.65829	0.00529	60.0%	40.0%
23-Feb-15	840	2.00E-08	0.00156	0.00270	4.45869	0.91035	0.00193	0.12161	0.00027	10.73490	0.75488	0.00490	60.6%	39.4%
2-Mar-15	1008	2.10E-08	0.00160	0.00304	4.23829	0.92154	0.00223	0.10599	0.00030	14.72109	0.69835	0.00558	60.0%	40.0%

40A														
				CATHODE					ANODE					
	Time	L	Rohm	Rc	Qc	nc	Rd c	Td c	Ra	Qa	na	(Rct + Rd)	% Rct	%Rd
	h	H	ohm	ohm	ad^(1-n).s^(n-1)		ohm	s	ohm	ad^(1-n).s^(n-1)				
20-Jan-15	0	2.40E-08	0.00146	0.00225	4.13077	0.96082	0.00172	0.09748	0.00023	8.45562	0.85764	0.00420	59.1%	40.9%
26-Jan-15	168	2.50E-08	0.00143	0.00221	4.68723	0.92545	0.00160	0.09219	0.00022	12.04889	0.79073	0.00403	60.4%	39.6%
2-Feb-15	336	2.50E-08	0.00143	0.00232	4.55228	0.93918	0.00198	0.09538	0.00023	11.43469	0.80657	0.00454	56.3%	43.7%
10-Feb-15	528	2.60E-08	0.00146	0.00261	5.40385	0.90150	0.00204	0.09535	0.00026	22.33790	0.69546	0.00491	58.4%	41.6%
17-Feb-15	696	2.00E-08	0.00147	0.00270	5.30786	0.91115	0.00229	0.09477	0.00027	16.01710	0.74572	0.00526	56.5%	43.5%
23-Feb-15	840	2.00E-08	0.00152	0.00264	4.97298	0.89602	0.00210	0.09374	0.00026	15.64266	0.71439	0.00500	58.1%	41.9%
2-Mar-15	1008	2.10E-08	0.00155	0.00330	4.99691	0.89967	0.00243	0.08065	0.00033	28.86628	0.62715	0.00606	59.9%	40.1%

50A														
				CATHODE					ANODE					
	Time	L	Rohm	Rc	Qc	nc	Rd c	Td c	Ra	Qa	na	(Rct + Rd)	% Rct	%Rd
	h	H	ohm	ohm	ad^(1-n).s^(n-1)		ohm	s	ohm	ad^(1-n).s^(n-1)				
20-Jan-15	0	2.40E-08	0.00145	0.00223	4.34013	0.95312	0.00171	0.07857	0.00022	9.15360	0.85792	0.00416	58.9%	41.1%
26-Jan-15	168	2.50E-08	0.00141	0.00191	3.94213	0.95161	0.00194	0.07809	0.00019	8.47646	0.83607	0.00405	52.0%	48.0%
2-Feb-15	336	2.50E-08	0.00142	0.00227	4.84795	0.92354	0.00219	0.07845	0.00023	17.50327	0.73807	0.00469	53.3%	46.7%
10-Feb-15	528	2.60E-08	0.00145	0.00261	5.64444	0.89472	0.00232	0.07583	0.00026	27.32565	0.67815	0.00518	55.3%	44.7%
17-Feb-15	696	2.00E-08	0.00146	0.00290	5.85211	0.89766	0.00259	0.07781	0.00029	19.62984	0.72501	0.00578	55.1%	44.9%
23-Feb-15	840	2.00E-08	0.00150	0.00271	5.39422	0.88454	0.00234	0.07543	0.00027	19.57543	0.69692	0.00532	56.0%	44.0%
2-Mar-15	1008	2.10E-08	0.00153	0.00362	5.75967	0.88276	0.00270	0.06323	0.00036	48.59591	0.57414	0.00668	59.6%	40.4%

60A															
				CATHODE					ANODE						
	Time	L	Rohm	Rc	Qc	nc	Rd c	Td c	Ra	Qa	na	(Rct + Rd)	% Rct	%Rd	
	h	H	ohm	ohm	ad^(1-n).s^(n-1)		ohm	s	ohm	ad^(1-n).s^(n-1)					
20-Jan-15	0	2.40E-08	0.00145	0.00206	3.71898	0.97266	0.00210	0.07134	0.00021	7.59123	0.88358	0.00436	51.9%	48.1%	
26-Jan-15	168	2.50E-08	0.00139	0.00224	5.57288	0.90593	0.00204	0.06442	0.00022	27.57376	0.71325	0.00450	54.7%	45.3%	
2-Feb-15	336	2.50E-08	0.00141	0.00240	5.44291	0.90819	0.00245	0.06600	0.00024	25.51862	0.70804	0.00509	51.9%	48.1%	
10-Feb-15	528	2.60E-08	0.00143	0.00286	6.57452	0.87516	0.00263	0.06188	0.00029	42.00719	0.63990	0.00577	54.5%	45.5%	
17-Feb-15	696	2.10E-08	0.00139	0.00301	7.12292	0.84869	0.00349	0.05503	0.00030	145.96419	0.42839	0.00681	48.7%	51.3%	
23-Feb-15	840	2.00E-08	0.00148	0.00291	6.03447	0.87135	0.00292	0.06112	0.00029	32.74367	0.64535	0.00611	52.3%	47.7%	
2-Mar-15	1008	2.00E-08	0.00152	0.00401	5.65710	0.90693	0.00364	0.05794	0.00040	34.91905	0.65239	0.00805	54.8%	45.2%	

70A														
				CATHODE					ANODE					
	Time	L	Rohm	Rc	Qc	nc	Rd c	Td c	Ra	Qa	na	(Rct + Rd)	% Rct	%Rd
	h	H	ohm	ohm	ad^(1-n).s^(n-1)		ohm	s	ohm	ad^(1-n).s^(n-1)				
20-Jan-15	0	2.40E-08	0.00143	0.00265	5.92425	0.90243	0.00194	0.04372	0.00027	26.38713	0.76546	0.00485	60.1%	39.9%
26-Jan-15	168	2.60E-08	0.00136	0.00273	7.00775	0.87004	0.00199	0.06570	0.00027	82.33329	0.55574	0.00500	60.1%	39.9%
2-Feb-15	336	2.50E-08	0.00139	0.00249	5.94129	0.89557	0.00296	0.05622	0.00025	40.19373	0.65971	0.00571	48.1%	51.9%
10-Feb-15	528	2.60E-08	0.00142	0.00281	6.07455	0.89409	0.00351	0.05808	0.00028	31.43248	0.67578	0.00660	46.9%	53.1%
17-Feb-15	696	2.00E-08	0.00140	0.00269	7.18666	0.84358	0.00504	0.04733	0.00027	324.35130	0.40557	0.00800	37.0%	63.0%
23-Feb-15	840	2.00E-08	0.00144	0.00263	6.92625	0.83506	0.00433	0.04319	0.00026	201.79814	0.44056	0.00722	40.0%	60.0%
2-Mar-15	1008	2.10E-08	0.00147	0.00408	6.10531	0.89568	0.00485	0.04419	0.00041	66.67187	0.55619	0.00934	48.1%	51.9%

80A														
				CATHODE					ANODE					
	Time	L	Rohm	Rc	Qc	nc	Rd c	Td c	Ra	Qa	na	(Rct + Rd)	% Rct	%Rd
	h	H	ohm	ohm	ad^(1-n).s^(n-1)		ohm	s	ohm	ad^(1-n).s^(n-1)				
20-Jan-15	0	2.40E-08	0.00143	0.00304	5.56301	0.92919	0.00179	0.06263	0.00030	16.52452	0.80720	0.00513	65.2%	34.8%
26-Jan-15	168	2.50E-08	0.00138	0.00283	7.18145	0.87725	0.00255	0.05481	0.00028	44.26465	0.67907	0.00566	55.0%	45.0%
2-Feb-15	336	2.50E-08	0.00138	0.00288	6.80223	0.88438	0.00330	0.04639	0.00029	50.88471	0.64400	0.00647	48.9%	51.1%
10-Feb-15	528	2.60E-08	0.00140	0.00331	7.27922	0.87462	0.00394	0.04100	0.00033	51.45396	0.63210	0.00758	48.0%	52.0%
17-Feb-15	696	2.10E-08	0.00138	0.00392	7.54768	0.87080	0.00509	0.03802	0.00039	67.49725	0.57451	0.00939	45.9%	54.1%
23-Feb-15	840	2.00E-08	0.00143	0.00345	6.83872	0.87129	0.00463	0.04042	0.00035	51.23947	0.60846	0.00843	45.1%	54.9%
2-Mar-15	1008	2.10E-08	0.00145	0.00409	6.31890	0.89338	0.00635	0.03501	0.00041	76.02331	0.55079	0.01085	41.5%	58.5%

90A														
				CATHODE					ANODE					
	Time	L	Rohm	Rc	Qc	nc	Rd c	Td c	Ra	Qa	na	(Rct + Rd)	% Rct	%Rd
	h	H	ohm	ohm	ad^(1-n).s^(n-1)		ohm	s	ohm	ad^(1-n).s^(n-1)				
20-Jan-15	0	2.50E-08	0.00141	0.00204	4.62372	0.92871	0.00338	0.04732	0.00020	72.74955	0.61300	0.00562	39.9%	60.1%
26-Jan-15	168	2.60E-08	0.00134	0.00298	7.38242	0.86716	0.00289	0.04138	0.00030	135.35839	0.51351	0.00617	53.1%	46.9%
2-Feb-15	336	2.50E-08	0.00137	0.00308	7.05920	0.88675	0.00390	0.03969	0.00031	59.95874	0.63466	0.00729	46.5%	53.5%
10-Feb-15	528	2.60E-08	0.00139	0.00330	7.11264	0.88452	0.00509	0.03677	0.00033	57.03441	0.63182	0.00873	41.6%	58.4%
17-Feb-15	696	2.00E-08	0.00139	0.00368	7.50695	0.87680	0.00698	0.02887	0.00037	54.07910	0.64629	0.01102	36.7%	63.3%
23-Feb-15	840	2.00E-08	0.00141	0.00332	6.91934	0.87303	0.00618	0.03330	0.00033	67.18106	0.59337	0.00983	37.1%	62.9%
2-Mar-15	1008	2.10E-08	0.00143	0.00370	6.00332	0.89586	0.00811	0.03260	0.00037	75.71038	0.55846	0.01218	33.4%	66.6%

100A														
				CATHODE					ANODE					
	Time	L	Rohm	Rc	Qc	nc	Rd c	Td c	Ra	Qa	na	(Rct + Rd)	% Rct	%Rd
	h	H	ohm	ohm	ad^(1-n).s^(n-1)		ohm	s	ohm	ad^(1-n).s^(n-1)				
20-Jan-15	0	2.40E-08	0.00142	0.00226	5.50654	0.91468	0.00363	0.03383	0.00023	38.96428	0.75673	0.00612	40.6%	59.4%
26-Jan-15	168	2.60E-08	0.00134	0.00239	6.39728	0.87674	0.00336	0.04057	0.00024	198.67424	0.44755	0.00598	43.9%	56.1%
2-Feb-15	336	2.50E-08	0.00136	0.00227	6.80116	0.87794	0.00555	0.03842	0.00023	154.25585	0.54381	0.00805	31.1%	68.9%
10-Feb-15	528	2.60E-08	0.00137	0.00218	6.62653	0.87968	0.00748	0.03921	0.00022	123.15042	0.55772	0.00988	24.3%	75.7%
17-Feb-15	696	2.10E-08	0.00135	0.00244	6.56543	0.87817	0.00978	0.04071	0.00024	117.93764	0.51636	0.01247	21.5%	78.5%
23-Feb-15	840	2.00E-08	0.00140	0.00216	6.31241	0.87375	0.00852	0.03663	0.00022	68.18287	0.60829	0.01089	21.8%	78.2%
2-Mar-15	1008	2.10E-08	0.00141	0.00234	5.64648	0.88784	0.01029	0.03627	0.00023	68.32489	0.57475	0.01286	20.0%	80.0%
3-Mar-15		2.00E-08	0.00143	0.00192	5.88734	0.86138	0.00948	0.03397	0.00019	70.27975	0.57512	0.01160	18.2%	81.8%

110A														
				CATHODE					ANODE					
	Time	L	Rohm	Rc	Qc	nc	Rd c	Td c	Ra	Qa	na	(Rct + Rd)	% Rct	%Rd
	h	H	ohm	ohm	ad^(1-n).s^(n-1)		ohm	s	ohm	ad^(1-n).s^(n-1)				
20-Jan-15	0	2.50E-08	0.00141	0.00265	5.79484	0.91377	0.00411	0.04127	0.00027	72.59230	0.64683	0.00703	41.5%	58.5%
26-Jan-15	168	2.50E-08	0.00137	0.00215	6.29724	0.89236	0.00438	0.03688	0.00022	67.67728	0.66448	0.00675	35.1%	64.9%
2-Feb-15	336	2.50E-08	0.00138	0.00249	7.21218	0.87361	0.00469	0.03010	0.00025	72.39457	0.64712	0.00743	36.9%	63.1%
10-Feb-15	528	2.60E-08	0.00139	0.00240	6.87737	0.87743	0.00645	0.03277	0.00024	70.27774	0.64059	0.00909	29.0%	71.0%
17-Feb-15	696	2.10E-08	0.00138	0.00202	6.40532	0.87260	0.00770	0.03766	0.00020	60.96909	0.62210	0.00992	22.4%	77.6%
23-Feb-15	840	2.00E-08	0.00140	0.00212	6.07284	0.87878	0.00883	0.03834	0.00021	60.30247	0.63040	0.01116	20.9%	79.1%
3-Mar-15	1008	2.00E-08	0.00140	0.00216	5.39269	0.88222	0.01054	0.03526	0.00022	60.58589	0.59433	0.01292	18.4%	81.6%

120A														
				CATHODE					ANODE					
	Time	L	Rohm	Rc	Qc	nc	Rd c	Td c	Ra	Qa	na	(Rct + Rd)	% Rct	%Rd
	h	H	ohm	ohm	ad^(1-n).s^(n-1)		ohm	s	ohm	ad^(1-n).s^(n-1)				
20-Jan-15	0	2.40E-08	0.00145	0.00187	6.47964	0.87739	0.00518	0.03245	0.00019	75.08446	0.73313	0.00724	28.4%	71.6%
26-Jan-15	168	2.60E-08	0.00134	0.00207	5.47519	0.91614	0.00524	0.04341	0.00021	118.64285	0.52554	0.00752	30.3%	69.7%
2-Feb-15	336	2.50E-08	0.00137	0.00208	6.74707	0.87831	0.00579	0.03283	0.00021	181.69328	0.54330	0.00808	28.3%	71.7%
10-Feb-15	528	2.70E-08	0.00135	0.00215	6.43048	0.88147	0.00786	0.03588	0.00021	181.95173	0.46669	0.01022	23.1%	76.9%
17-Feb-15	696	2.00E-08	0.00136	0.00188	6.17642	0.88471	0.00909	0.03488	0.00019	72.84013	0.60818	0.01116	18.5%	81.5%
23-Feb-15	840	2.00E-08	0.00137	0.00183	5.64191	0.88914	0.00938	0.04155	0.00018	72.84013	0.60818	0.01140	17.7%	82.3%
3-Mar-15	1008	2.00E-08	0.00138	0.00190	5.38768	0.88319	0.01095	0.03416	0.00019	72.23476	0.57021	0.01304	16.0%	84.0%

References

Andrienko, Denis, Cyclic Voltammetry. 2008. http://www2.mpip-mainz.mpg.de/~andrienk/journal_club/cyclic_voltammetry.pdf (accessed January 2015).

Bambase Manolito, E. Handout F. Constants for Vapor Pressure Calculation Using Antoine Equation. http://che31.weebly.com/uploads/3/7/4/3/3743741/handout_f-antoineconstants.pdf (accessed Jan 19, 2015).

Bonnet, Caroline. Personal communication. 2015.

Cooper, Kevin. In situ PEM Fuel Cell Electrochemical Surface Area and Catalyst Utilization Measurement. *Fuel Cell Magazine*. Scribner Associates Inc. Jan/Feb 2009. http://www.scribner.com/files/tech-papers/Scribner-on-ECSA-Fuel-Cell-Magazine-2009.pdf.

Fuel Cell diaphragm/ with electrode. Paxi Tech. http://www.directindustry.com/prod/paxitech/fuel-cell-diaphragms-electrode-126393-1527697.html.

Fuel Cell Technologies. Office.Energy.gov. http://energy.gov/eere/fuelcells/fuel-cell-technologies-office (accessed Feb 23, 2015).

Gamry Instruments. Basics of Electrical Impedance Spectroscopy. http://www.gamry.com/application-notes/basics-of-electrochemical-impedance-spectroscopy/ (accessed Jan 22, 2015).

Gouws, Shaun. Voltammetric Characterization Methods for the PEM Evaluation of Catalysts. Intech, 2012. (accessed Jan27, 2015). http://cdn.intechopen.com/pdfs-wm/40135.pdf.

Hartnig, Christoph and Christina Roth. *Polymer electrolyte membrane and direct methanol fuel cell technology*. Volume 1. Cambridge, UK: Woodhead Publishing, 2012.

Kumpulainen, Heikki, Terttu, Peltonen, Ulla, Koponen, Bergelin, Mikael, Valkiainen, Matti, and Wasberg, Mikael. "In situ voltammetric characterization of PEM fuel cells catalyst layers". VTT Research Notes 2137. ESPOO 2002. (accessed January 2015) http://www2.vtt.fi/inf/pdf/tiedotteet/2002/T2137.pdf.

Larminie, James and Andrew Dicks. Fuel Cell Systems Explained. 2nd ed. Chichester, West Suffsex: J.Wiley, 2003.

Lapicque, Francois. Personal communication. 2015.

Metrohm Autolab B.V. Autolab Application Note EC08.
http://sis.nlm.nih.gov/enviro.html
(accessed Mar 3, 2015).

Orazem, Mark and Tribollet, Bernard. Electrochemical impedance spectroscopy, Hoboken, N.J.: Wiley, 2008.

Polarization Curve. Corrosionpedia [Online]; Janata Interactive Inc., 2015.
http://www.corrosionpedia.com/definition/898/polarization-curve (accessed January 22, 2015).

Sundmacher, Kai. *Advances in Chemical Engineering;* Sundmacher, Kai, Ed.; Elsevier Inc.: San Diego, 2012; Vol. 41; p 126-135, 369-372.

Wu, Jinfeng, Yuan, Xiao-Zi, and Wang, Haijiang."Cyclic Voltammetry". In *PEM Fuel Cell Diagnostic Tools*; Ed.; Wang, Haijiang, Yuan, Xiao-Zi and Li, Hui. CRC Press: Boca Raton, FL, 2012; pp 71-84.

Zhang, Shengsheng, Yuan, Xio-Zi, and Wang, Haijiang. Linear Sweep Voltammetry. In *PEM Fuel Cell Diagnostic Tools*; Ed.; Wang, Haijiang, Yuan, Xiao-Zi and Li, Hui. CRC Press: Boca Raton, FL, 2012; pp 87-100.